

The Global Distribution of Ultra-Low-Frequency Waves in Jupiter's Magnetosphere

H. Manners¹, A. Masters¹

¹Space and Atmospheric Physics Group, Blackett Laboratory, Imperial College London, London, UK

Key Points:

- We used heritage magnetometer data to produce the first global statistical survey of ultra-low-frequency waves in Jupiters magnetosphere.
- The waves have periods spanning ~5-60 min, dominated by ~15, ~30 and ~40 min pulsations, consistent with periods reported in the literature.
- The population of waves have a diverse spatial distribution, indicating multiple driving mechanisms and several distinct resonant cavities.

Abstract

Jupiter's giant magnetosphere is a complex system seldom in a configuration approximating steady state, and a clear picture of its governing dynamics remains elusive. Crucial to understanding how the magnetosphere behaves on a large scale are disturbances to the system on length-scales comparable to the cavity, which are communicated by magnetohydrodynamic waves in the ultra-low-frequency band (<1 mHz). In this study we used magnetometer data from multiple spacecraft to perform the first global heritage survey of these waves in the magnetosphere. To map the equatorial region, we relied on the large local-time coverage provided by the Galileo spacecraft. Flyby encounters performed by Voyager 1 & 2, Pioneer 10 & 11 and Ulysses provided local-time coverage of the dawn sector. We found several hundred events where significant wave power was present, with periods spanning ~ 5 -60 min. The majority of events consisted of multiple superposed discrete periods. Periods at ~ 15 , ~ 30 and ~ 40 min dominated the event-averaged spectrum, consistent with the spectra of quasi-periodic pulsations often reported in the literature. Most events were clustered in the outer magnetosphere close to the magnetopause at noon and dusk, suggesting that an external driving mechanism may dominate. The most energetic events occurred close to the planet, though more sporadically, indicating an accumulation of wave energy in the inner magnetosphere or infrequent impulsive drivers in the region. Our findings suggest that dynamics of the system at large scales is modulated by this diverse population of waves, which permeate the magnetosphere through several cavities and waveguides.

1 Introduction

The magnetosphere of Jupiter is the largest structure embedded inside the heliosphere, yet an understanding of its dynamics remains elusive. The magnetospheric cavity is host to many dynamical processes occurring on energy-scales exceeding their terrestrial equivalents by several orders of magnitude (Bolton et al., 2002; Bagenal & Delamere, 2011a; B. Mauk & Bagenal, 2013). This complex environment represents an analogue to high-energy astrophysical environments that is relatively local to Earth, offering a vast natural laboratory to test plasma-physics theory. A persistent ongoing problem is an incomplete understanding of how energy and momentum are exchanged between different regions, especially between the magnetosphere and ionosphere. This prohibits a clear picture of global dynamics, which are markedly different from the solar-

44 wind-dominated planetary magnetospheres (Barbosa et al., 1979; K. Khurana et al., 2004;
45 Went et al., 2011; Achilleos et al., 2015). This is because Jupiter rotates on its axis in
46 just ten hours; this fast rotation, coupled with the planet’s large intrinsic magnetic field,
47 means that the magnetosphere derives the majority of its energy and momentum bud-
48 get from the planet’s core via electromagnetic coupling. By contrast, the magnetospheres
49 of the other magnetized planets are driven mainly by the solar wind, and so ultimately
50 by the Sun.

51 The aurora at Jupiter’s poles provide a proxy for this novel high spatial- and temporal-
52 variability. Results from the JUNO spacecraft have shown the associated particle flux
53 and electromagnetic emissions to be even more complex than previously thought, sug-
54 gesting equally complex dynamics out in the magnetosphere which drive these emissions
55 (Allegrini et al., 2017; Clark et al., 2017; B. H. Mauk et al., 2017a, 2017b; Gershman et
56 al., 2019). As argued recently by Saur et al. (2018), the long-standing paradigm of a quasi-
57 steady-state magnetosphere dominated by static, powerful field-aligned-currents (FACs)
58 has fallen into question, given that these FACs have been observed to be weaker than
59 anticipated, and filamentary in structure, with evidence of stochastic acceleration pro-
60 ducing broadband auroral signatures (Ebert et al., 2017; Kotsiaros et al., 2019). It is likely
61 that time variable phenomena in the magnetosphere are responsible for the fine struc-
62 ture of the aurora, little of which has been studied in detail.

63 Prominent among these unexplained temporal phenomena are ubiquitous quasi-
64 periodic oscillations (QPOs) in the ultra-low-frequency (ULF) band. Reports span mul-
65 tiple data sets and cover a wide range of periods, encompassing $\sim 1 - 100$ min, though
66 concentrated around 10 - 60 min. The full list of observations span modulations in the
67 X-Ray, infra-red (IR) and ultra-violet (UV) auroral emissions (Gladstone et al., 2002;
68 Nichols et al., 2017; Dunn et al., 2017; Watanabe et al., 2018), magnetic field (K. Khu-
69 rana & Kivelson, 1989), radio waves (MacDowall et al., 1993; Hospodarsky et al., 2004;
70 Arkhypov & Rucker, 2006; Kimura et al., 2011, 2012) and energetic particle flux (Anagnostopoulos
71 et al., 2001; Karanikola et al., 2004). There also appear to be several preferential ULF
72 periods, often referred to in the literature as “magic frequencies”, around ~ 15 , ~ 30 and
73 ~ 40 min (also sometimes called QP-15, QP-30 and QP-40). Several studies have surveyed
74 ULF wave activity in the middle magnetosphere using a subset of the available data and
75 a sub-band of the ULF spectrum (e.g. Tsurutani et al. (1993); Schulz et al. (1993); Petkaki
76 and Dougherty (2001); Wilson and Dougherty (2000); Russell et al. (2001)), and collectviely

77 found significant wave power within 1-60 min. A recent comprehensive review of the topic
78 by Delamere (2016) contains more detail on the history of research featuring QPOs at
79 Jupiter.

80 The driving mechanisms of these phenomena have remained a mystery for decades.
81 However, it is well established that the majority of QPOs are associated with magnetic
82 field lines that map to the middle- and outer-magnetosphere, and Alfvénic activity. When
83 the magnetosphere is perturbed on a length-scale similar to the size of the system, mag-
84 netohydrodynamic (MHD) waves in the fast-compressional and Alfvén modes communi-
85 cate the new stress distribution imposed by the perturbation. MHD waves in the ULF
86 band travelling at typical Alfvén speeds have length-scales comparable to the scale of
87 the magnetosphere, and so an Alfvénic resonance of the magnetic field may be respon-
88 sible for the observed QPOs. The quasi-periodic behaviour of QPOs is consistent with
89 non-stationary resonances or localized resonances created by the complex structure of
90 the magnetosphere.

91 ULF waves in the terrestrial magnetosphere have received significant attention in
92 the literature. Early work demonstrated a mechanism for exciting a global resonance mode
93 of the magnetosphere known as a field-line-resonance (FLR), whereby propagating fast-
94 mode ULF waves excite magnetic field lines at their natural frequencies. Trans-hemispheric
95 standing Alfvén waves (SAWs) are subsequently established via a transfer of energy from
96 compressional to Alfvén modes in the resonance region (Tamao, 1965; D. J. Southwood,
97 1974; Chen & Hasegawa, 1974; D. Southwood & Hughes, 1983). D. J. Southwood and
98 Kivelson (1986) and K. Khurana and Kivelson (1989) postulated that a similar mech-
99 anism is active at Jupiter, but that the waves are likely confined to the equatorial re-
100 gion by the distribution of plasma along the field line, which is dominated by the equa-
101 torial plasma-sheet. Regions away from the plasma sheet are plasma-depleted and so the
102 Alfvén speed rapidly becomes relativistic. The wave therefore spends the majority of its
103 transit time in the plasma sheet, and so to first order the transit time is determined by
104 the properties of this region.

105 Manners et al. (2018) showed that QPOs at Jupiter are well described to first or-
106 der by SAWs and, given conservative variations in the plasma sheet Alfvén speed and
107 thickness, the periods span 1 - 60 min for the first half-dozen harmonics. These SAWs
108 can be depicted in 1D as transverse displacements on a ‘magnetic string’, where mag-
109 netic tension acts as a restoring force, and the ionospheric footprints represent fixed bound-

aries of the string. Multiple harmonics can be established in superposition along the field line, provided the compressional wave forcing the resonance has a bandwidth spanning several harmonic frequencies of the field line. The magnetosphere can therefore be treated as an infinite set of independent resonators, each with its own natural frequency and so its own set of harmonics (Wright & Mann, 2013). A case study by Manners and Masters (2019) presented a multiple-harmonic SAW confined to the plasma sheet in the jovian magnetotail, with spectral properties consistent with frequently observed QPO periods. This demonstrates that at least a sub-set of QPOs are described by SAWs.

Progressing from these theories to a fuller understanding of ULF waves at Jupiter requires a heritage survey of all the available data to capture the systematic spatial distribution of QPOs in the magnetosphere. Here we present such a heritage survey, using the in-situ magnetic field data from multiple spacecraft. In section 2 we discuss the data used in the survey, and an algorithm used to analyse the data and identify ULF events of interest. In section 3 we present the results of the survey, featuring the spatial distribution of QPOs. In section 4 we discuss potential drivers of SAWs at Jupiter and the implications they have for energy and momentum transfer through the system.

2 Spacecraft Data and an Algorithm for Identifying ULF Pulsations

2.1 Magnetometer Data from Multiple Encounters with Jupiter

To date, seven spacecraft have crossed the magnetopause and transited the jovian magnetosphere: Pioneer 10 & 11, Voyager 1 & 2 and Ulysses flew by the system, Galileo was the first dedicated orbiter, and JUNO is currently in orbit at the time of writing. The majority of the pre-JUNO spacecraft trajectories were close to the equatorial plane, with the exception of Ulysses and Pioneer 11, which traversed the dusk-ward southern-hemisphere and the noon-sector northern-hemisphere, respectively. We expect ULF wave-power and any SAWs to be concentrated in the equatorial plasma-sheet, and so near-equatorial data are of particular interest. Data from Galileo covered a broad span of local time, except for dawn; data from the flybys contributed the majority of coverage of this region.

While Galileo provided the most data, the spacecraft experienced significant telemetry problems after the high-gain antenna sustained damage. Measurements from all instruments were downlinked at a variable data-rate throughout the orbital tour, with the exception of high-interest intervals such as moon flybys. Additionally, the Plasma Sci-

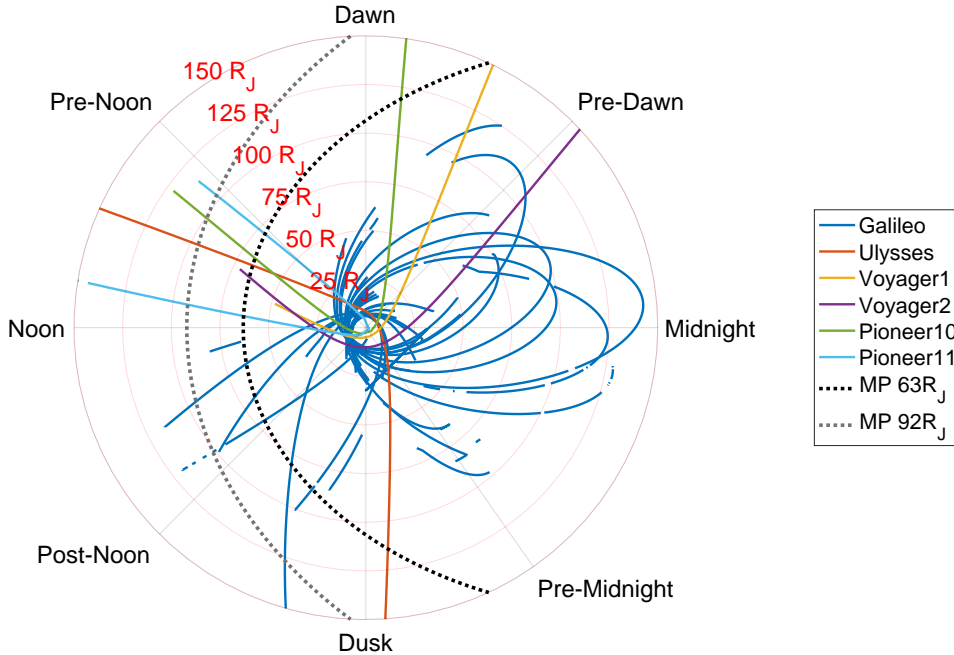


Figure 1. Portions of spacecraft trajectories during intervals where magnetometer data was suitable for inclusion in the survey, shown in equatorial cross-section. Data are omitted where the sampling cadence falls below the 2 min threshold required to capture the full ULF spectrum. The dotted lines show the bi-modal statistical position of the magnetopause (Joy et al., 2002).

142 ence instrument (PLS) (Frank et al., 1992) suffered damage preventing analysis of the
 143 thermal electrons, and poor pointing constraints limited the quality of calculated plasma
 144 parameters for the ions (Bagenal et al., 2016). We therefore limit our survey to exclu-
 145 sively using magnetometer data. As the primary focus of the survey is to inspect global
 146 resonance modes inside the magnetosphere, we excluded data measured outside the mag-
 147 netopause, though ULF power in the magnetosheath or the solar wind may warrant in-
 148 spection in a later study. Detailed information about the magnetometer instrument de-
 149 sign on each spacecraft can be found in Van Allen et al. (1974); Acuna and Ness (1980);
 150 Kohlhase and Penzo (1977); Smith et al. (1992); Kivelson et al. (1992), listed in chrono-
 151 logical order of when the spacecraft encountered Jupiter. As JUNO is in a polar orbit
 152 it spends minimal time close to the plasma sheet, and so we do not include these data
 153 in the survey.

154 The nominal cadence of magnetometer data throughout the Galileo mission was
 155 24 s, but for portions of the tour the rate was significantly lower. A compromise is re-
 156 quired between capturing the full ULF frequency band and retaining as much data as

157 possible. To reach this compromise we imposed a cut-off in cadence above which low data-
 158 rates effectively constitute a data-gap. The lowest resolvable period τ_{min} is given by the
 159 Nyquist condition $\tau_{min} = 2\tau_s$, where τ_s is the sampling cadence. We chose a cut-off at
 160 a sampling cadence of 2 min, which retains 97.5% of data from the Galileo magnetome-
 161 ter, and gives a lower bound on the resolvable periods of 4 min. Given that the lowest
 162 observed periods in QPOs were ~ 2 -3 min, this eliminates only the extreme lower-limit
 163 of the range of interest, which in future could be made the subject of a dedicated study
 164 using a subset of the available data. We downsampled the remaining data to the modal
 165 cadence over each day to ensure that spectral analysis was performed at a consistent data
 166 rate. Magnetometer data from Pioneer 10 & 11, Voyager 1 & 2 and Ulysses required min-
 167 imal processing, as in each case magnetic field vectors were sampled at least once per
 168 min, allowing the full ULF band to be analysed. The choice of a 4 min lower-bound on
 169 the ULF spectrum also avoids the issue of detecting spin-tones of the rotating spacecraft
 170 (Galileo rolled with a 19 s spin-period, and the other spacecraft were similar except for
 171 Voyager 1 & 2, which did not roll). Figure 1 shows an equatorial-plane projection of the
 172 trajectories of the six spacecraft included in the survey. The data shown are those which
 173 were measured with a sufficient sampling cadence less than 2 min. Any gaps in the tra-
 174 jectories correspond to times when the magnetometers were offline or in low-data-rate
 175 modes. Once processed, the data were then passed through an algorithm for analysis,
 176 where intervals of interest in ULF activity could be identified.

177 2.2 An Algorithm for Identifying ULF Waves

178 We used an algorithm to survey the large volume of data and construct a catalogue
 179 of ULF ‘events’. Due to the highly dynamic nature of the magnetosphere and the vari-
 180 able digitization-noise floors of each magnetometer, field perturbations with amplitudes
 181 below 1 nT cannot be unambiguously separated from statistical fluctuations for the en-
 182 tire dataset. To ensure robust results we only identified pulsations with amplitudes of
 183 several nT during relatively quiet magnetospheric conditions, a process that we now de-
 184 scribe in detail.

185 The data were analysed using a framework presented in Fig. 2. During this inter-
 186 val Galileo traversed the tail plasma-sheet close to midnight, 50-60 R_J from Jupiter. The
 187 magnetic field data in spherical coordinates corotating with Jupiter (known as Jupiter
 188 System III) in Fig. 2.a) show perturbations of periods on the order tens of min super-

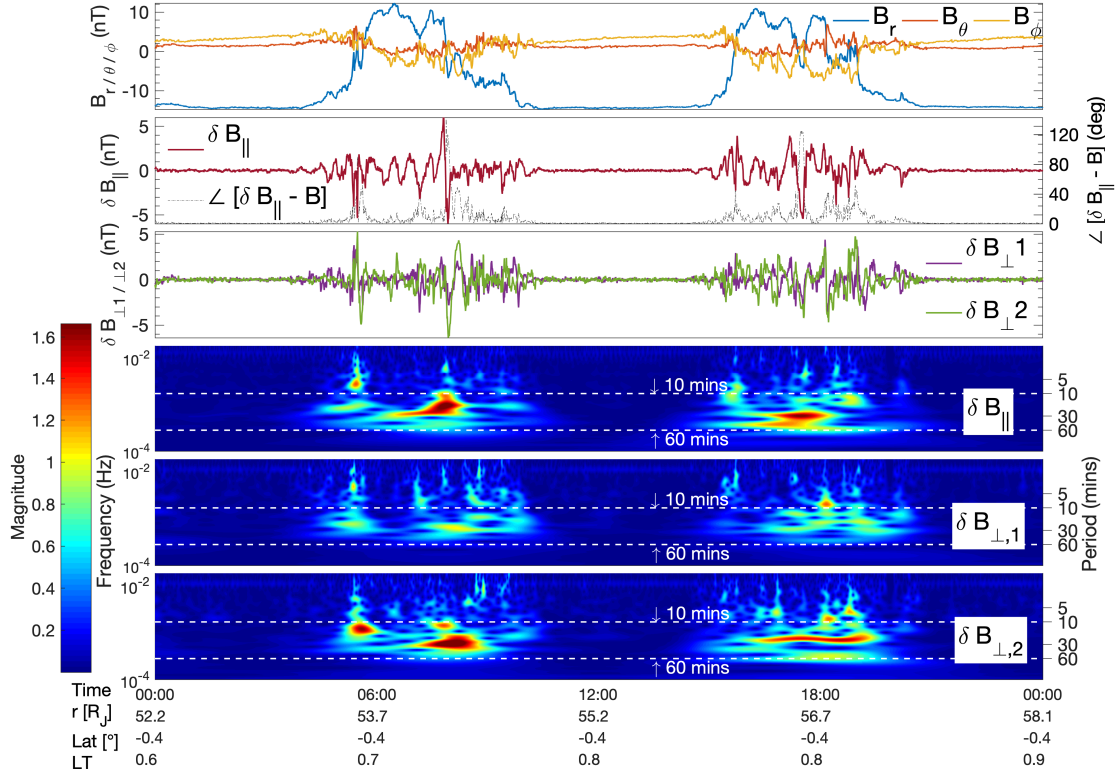


Figure 2. Analysis framework showing magnetometer data from the Galileo spacecraft during 13th-14th September 1996. a) Magnetic field data in spherical system III coordinates. b) Field-aligned component of the mean-field-aligned (MFA) magnetic field residual (red line), and angle of deviation between the local magnetic field vector and the computed MFA unit vector (black dashed line). c) Both transverse components of the MFA magnetic field residual. d)-f) Continuous wavelet transforms for the field-parallel and field-transverse MFA magnetic field residuals, respectively. The white dotted-lines in d-f) demonstrate that most of the ULF power is concentrated within 10 and 60 min.

189 posed on top of the long-timescale evolution of the field. To inspect these small-amplitude
 190 perturbations, we rotated the data into mean-field-aligned (MFA) coordinate system (see
 191 K. Khurana and Kivelson (1989); Manners et al. (2018)), using a moving-average win-
 192 dows of 60 min to produce a principal unit vector \hat{b}_{\parallel} aligned with the average background
 193 magnetic field. The unit vectors $\hat{b}_{\perp,1}$ and $\hat{b}_{\perp,2}$ complete a right-handed orthogonal set
 194 and are transverse to the mean field. The 60-min background field is then removed, pro-
 195 ducing the MFA residual magnetic field components δb_{\parallel} , $\delta b_{\perp,1}$ and $\delta b_{\perp,2}$, shown in fig-
 196 ure 2.b-c). Further examples of intervals analysed using this framework in different parts
 197 of the magnetosphere can be found in Supplementary Materials.

Transient or impulsive phenomena unlikely to be MHD waves, or changes in instrumentation dynamic ranges, occur often. To filter out these intervals we used a threshold in the normalized moving-variance σ of the magnetic field magnitude

$$\sigma(B_i) = \frac{1}{2wB_i} \sum_{j=-w}^w (\bar{B}_{i+j} - \bar{B}_i)^2, \quad (1)$$

198 where w is the window half-width and \bar{B}_i is the mean magnetic field over a 60 min in-
 199 terval. We neglected intervals when σ_{B_i} exceeded 1 nT, using a moving-variance win-
 200 dow half-width 10 min. This filter is particularly effective for isolating Alfvénic activ-
 201 ity, as Alfvén waves do not perturb the magnetic field magnitude.

202 There are also geometric constraints to consider. The radial distension of the mag-
 203 netic field is greatest near the magnetic equator in the middle magnetosphere, due to cen-
 204 trifugal forces acting on the equatorially-confined plasma. This causes reversals in the
 205 radial and azimuthal components of the magnetic field over a spatial-length-scale on the
 206 order of several jovian radii. The velocity of each spacecraft with respect to the plasma-
 207 sheet-normal direction was variable, but the average time taken to traverse the plasma
 208 sheet was around 30 min. This timescale is shorter than the width of the moving win-
 209 dow used to obtain the MFA basis vectors; in this region the fidelity of these vectors in
 210 capturing the mean-field direction is poor, and they are no longer field-parallel/transverse
 211 across the whole interval. In these instances, field-aligned and Alfvénic activity are im-
 212 possible to distinguish, and so they were removed from the analysis. To remove these
 213 intervals, we calculated the angle of rotation between the local magnetic field vector and
 214 the computed instantaneous MFA unit vector, which is shown by the black dotted line
 215 in Fig. 2b). We imposed a limit on the acceptable angle of deviation to a cone-angle sub-
 216 tending 45 degrees from the local magnetic field vector. This constraint almost invari-
 217 ably removes intervals where the spacecraft is travelling through the centre-most region
 218 of the plasma sheet, which is expected to be the primary locus of ULF wave-power. How-
 219 ever, while the latitudinal plasma-density gradient is large, the waves are unlikely to be
 220 perfectly confined to the centre-most region. Consequently, this central-plasma-sheet ‘blind-
 221 spot’ is assumed to diminish the number of identified events without introducing bias
 222 to the resulting distribution of wave periods.

223 Fig. 2.b-c) show several enhancements in the amplitudes of magnetic field pertur-
 224 bations while Galileo crossed the equatorial plasma sheet. To obtain spectral informa-
 225 tion of the wave packets in frequency-time space, we computed the wavelet transforms
 226 of each MFA residual component using a Morlet wavelet (Gaussian-modulated plane-

227 wave), the results of which are shown in Fig. 2d-f. The region where edge effects are large
 228 is beyond the limits of the plotted data. The wavelet transform offers superior simulta-
 229 neous localization of non-time-stationary fluctuations in both frequency and time com-
 230 pared to other spectral methods, a capacity crucial for identifying QPOs, which are time-
 231 variable by nature. We nevertheless validated the results of the wavelet transform by com-
 232 parison to fast-Fourier-transform (FFT) and Lomb-Scargle spectra (see Supplementary
 233 Materials for examples).

To classify an ULF-active interval as an event, we used a threshold in the wavelet
 power integrated over the ULF band, which we call the ULF bandpower P_{ULF} , defined
 as

$$P_{ULF} = \frac{1}{\nu_{max} - \nu_{min}} \int_{\nu_{min}}^{\nu_{max}} P(\nu) \delta\nu, \quad (2)$$

234 where ν is frequency, P is power spectral density and $\nu_{min/max}$ are the minimum and
 235 maximum frequencies of the ULF band. We set the threshold as twice the daily mean
 236 bandpower. The longest resolvable period is given by the length of the time series, and
 237 so to capture the full ULF band up to 60 min, we considered only events where this thresh-
 238 old was exceeded for longer than an hour. Within each event any statistically significant
 239 discrete maxima in power were identified. We used Monte-Carlo simulations of the mag-
 240 netic field data during each interval of interest to perform the significance test at a 95%
 241 confidence threshold, using 10,000 random reshuffles of the data, where we assumed the
 242 background spectrum is well-approximated by a red-noise process (Torrence & Compo,
 243 1998). Any intervals where power at a given period exceeded this significance level are
 244 hereafter referred to as significant periods.

245 The spectra of waves identified by the algorithm are subject to doppler shift, due
 246 to the relative motion of the spacecraft and the plasma rest frame. A simple calculation
 247 of the frequency shift introduced by over range of spacecraft velocities on waves with rest-
 248 frame periods between ~ 10 -60 mins shows that the effect is minimal, introducing a typ-
 249 ical shift of a few mins, and around 10 mins in the extreme. As the availability of bulk-
 250 velocity measurements from plasma moments is very limited, and a shift of several mins
 251 is small compared to the 10-60 min range of interest, we neglect this effect from our analysis—
 252 though the reader should remain aware of this bias.

253 The framework outlined above was applied to the magnetometer data from all six
 254 spacecraft, resulting in a catalogue of events of at least an hour in duration, with at least

255 one statistically significant enhancement in ULF power, providing the first global dis-
256 tribution of ULF waves in the magnetosphere.

257 **3 Survey Results and Analysis**

258 We found a combined total of around 650 events where significant ULF power was
259 present, mostly in the Galileo data. The duration of events peaked at 1 hour and most
260 events were 1-3 hours in duration, with a minority lasting up to 8 hours. As events shorter
261 than 1 hour were included in the survey were excluded from the survey, it is likely that
262 many more events exist in the data, which can be the subject of a future study on shorter-
263 period ULF waves. The average MFA angle of deviation during events was ~ 10 degrees,
264 confirming the success of the quality control measures imposed by the selection algorithm.
265 For more details, the interested reader may refer to the Supplementary Material.

266 The large number of events provides far greater spatial and spectral detail than pre-
267 vious studies. An analysis of the full extent of the information spans a wide range of top-
268 ics at various spatial scales, and is best explored in separate future works. The domi-
269 nant outstanding question at the time of writing regarding these waves is their effect on
270 energy flow through the magnetosphere, and their connection with the quasi-periodic sig-
271 natures observed throughout the literature. Therefore in the following sections we will
272 focus on the implications of the sampled distribution for large-scale magnetospheric dy-
273 namics.

274 In the events successfully identified, power was predominately concentrated in the
275 field-transverse components, but several hundred field-parallel events were also identi-
276 fied. The field-parallel events are difficult to interpret unambiguously, so we focus on the
277 field-transverse events, which can be reasonably assumed to be caused by Alfvén waves
278 and therefore representative of natural periods of the system in each region. Fig. 3 a)
279 through d) show several histograms of the field-transverse events in an equatorial-plane-
280 projection: a) the total dwell-time of spacecraft in each bin; b) the ULF bandpower av-
281 eraged over the events in each bin; c) the fraction of total time the spacecraft spent in
282 each bin when significant ULF wave-power was present; and d) the same as c) but for
283 the subset of events where only one significant period was present. Unsampled regions
284 are shown in white, and inactive regions where no significant ULF wave-power was de-
285 tected are shown in grey.

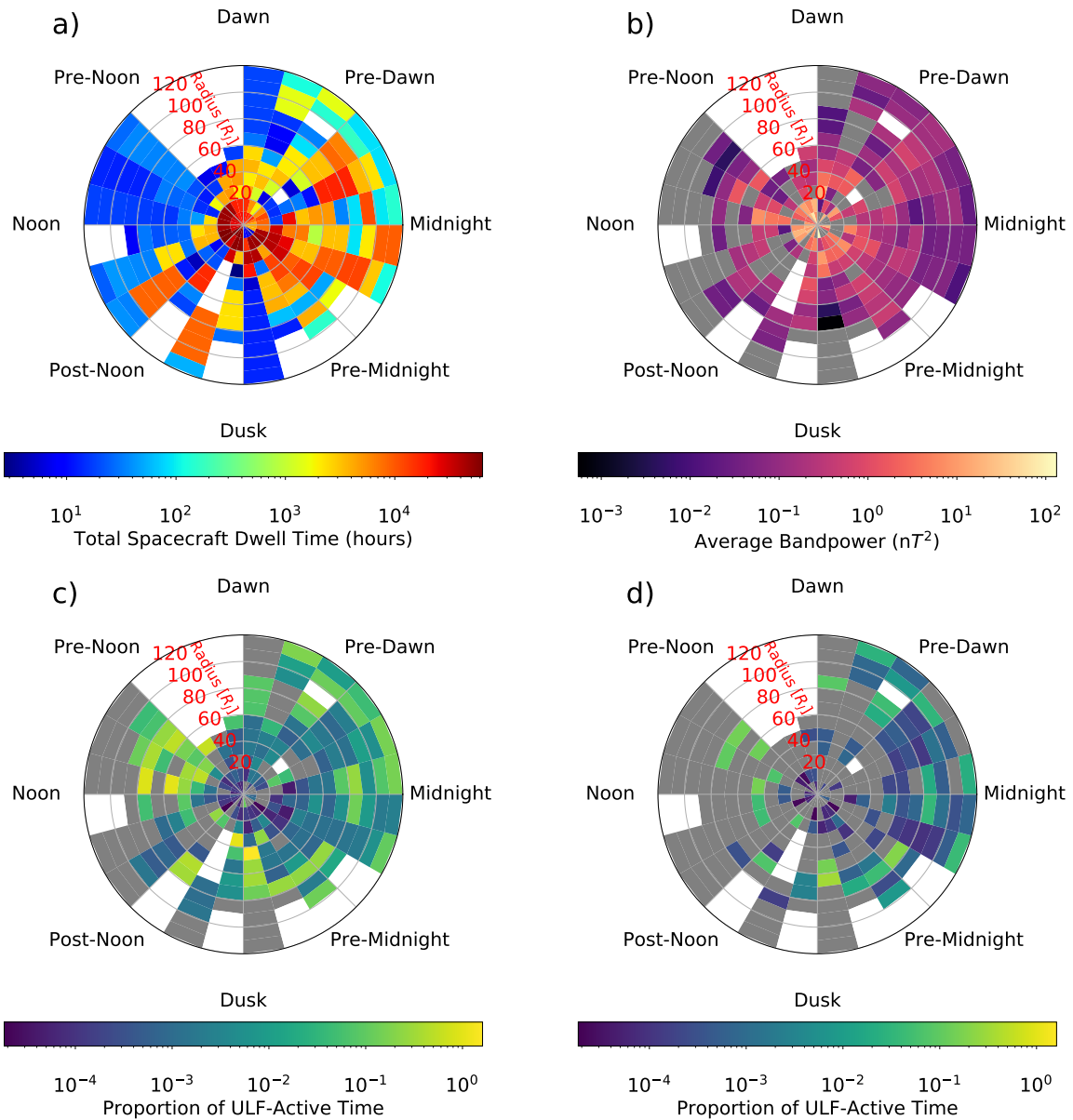


Figure 3. Histograms using field-transverse events gathered using data from all the spacecraft magnetometers, in an equatorial-plane projection: a) the total time spacecraft spent in each bin; b) the ULF bandpower averaged over the events in each bin; c) the proportion of time spacecraft spent in each region where significant ULF-activity was observed; d) same as c) for the subset of events where only a single significant period was observed. White bins signify where there are no available data, and grey bins signify regions where spacecraft visited but observed no events.

286

The ULF-active proportion of spacecraft dwell-time in Fig. 3c) demonstrates ULF waves occur most often in the outer magnetosphere, especially in the noon sector and

287

288 along the dusk flank. There is also regular activity in the magnetotail, where events with
 289 only a single significant period are concentrated, and where there also appears to be a
 290 dawn/dusk asymmetry in the bandpower (see Fig. 3d). Globally the majority of ULF
 291 activity appears to consist of multiple simultaneous discrete periods.

292 The distributions of periods in different components is shown in Fig. 4. Periods
 293 span the full 5 - 60 min observed in the literature, and there is suggestion of peaks con-
 294 sistent with the ‘magic frequencies’ QP-15, QP-30 and QP-40. The 30 min period ap-
 295 pears to dominate, and there also may be an intermediate ~ 35 min period. The QP-
 296 15 period appears to be spread more widely over 10-20 min than one discrete period, con-
 297 sistent with the 10-20 min ULF power found by K. Khurana and Kivelson (1989); these
 298 periods also have a systematically smaller power than 30 min and 40 min periods, and
 299 mostly appear only during events where multiple simultaneous periods were observed.
 300 The field-transverse and field-parallel events have periods largely coincident in time and
 301 space, consistent with compressional-wave driven FLRs, where energy is being transferred
 302 from fast-mode to the resonant Alfvén mode.

303 The majority of events field-transverse events showed the same significant spectral
 304 behaviour in both transverse components, but there is some evidence of independent de-
 305 coupled periods in the minority of cases; this may also be due to only one field-transverse
 306 component being present, caused by linearly polarized waves (see Fig. 2 in Supplemen-
 307 tary Materials).

308 Fig. 5 shows the distribution of periods in local-time for all the field-transverse events.
 309 The 30 min period is prominent in all local-time sectors, as is the 40-min period, though
 310 the latter appears most prominent in the dusk sector. There is a noticeable dawn-dusk
 311 asymmetry in the distributions: the dawn sector is skewed towards periods less than 30
 312 min, and the dusk sector is skewed towards periods longer than 30 min.

313 Localized deviations from the global distribution of periods are evident in several
 314 places: Fig. 6 compares the region of the plasma torus at Io’s orbit with the region close
 315 to the magnetopause at the sub-solar point. The broadband periods close to the plasma
 316 torus appear to consist of three harmonics at ~ 30 , 60 and 90 min, whereas the distri-
 317 bution close to the dayside magnetopause is much more narrowband and centred around
 318 30 min. The MFA magnetic field residuals shown in Fig. 6c) and d), and their respec-
 319 tive wavelet transforms in e) and f), are representative of the two regions. Events close
 320 to the torus are variable in profile, whereas the outer magnetospheric signals have a more

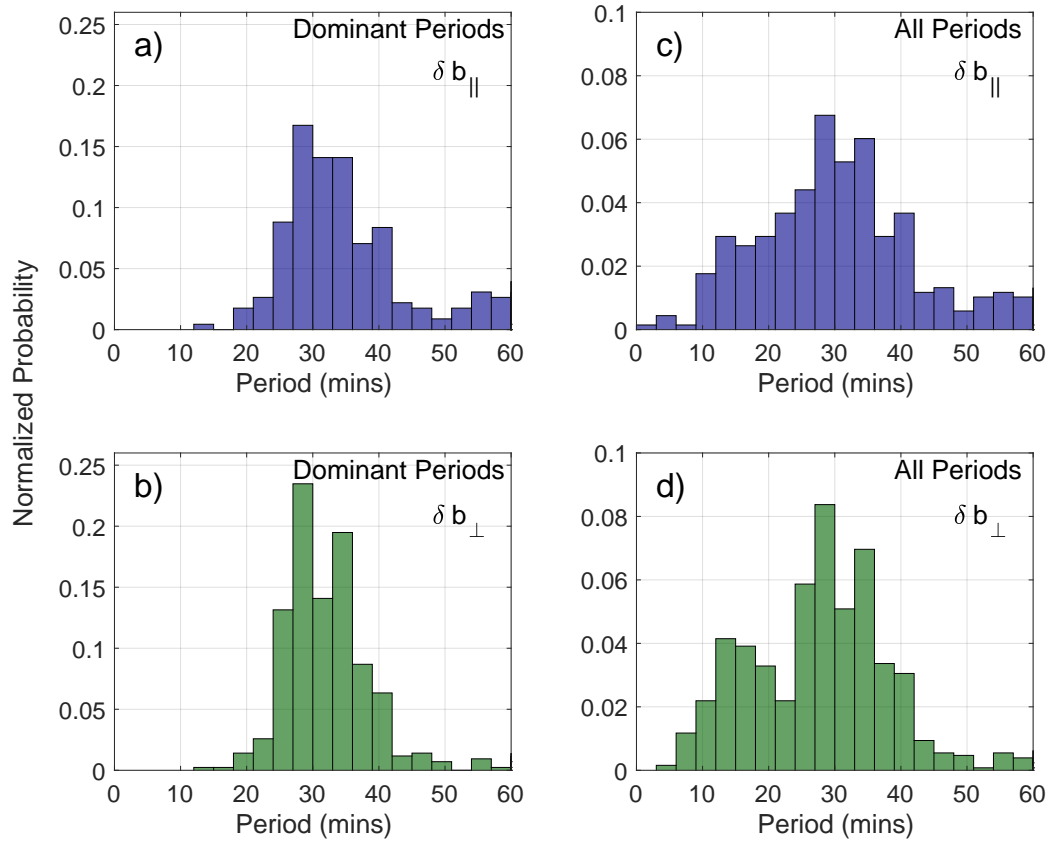


Figure 4. Normalized histograms of significant periods during all events identified in the survey: a) the distribution of events where only one significant period was identified in the field-parallel component or the dominant period when multiple significant periods were identified in the field-parallel component; b) same as a) for the field-transverse components; c) the distribution of all significant periods of events in the field-parallel component; d) same as c) for the field-transverse components. The 15 min, 30 min and 40 min ‘magic frequencies’ are evident in d), and the 30 min periods appears to dominate throughout.

321 regular ‘saw-tooth’ profile, which could possibly indicate a more homogeneous region or
 322 monochromatic source.

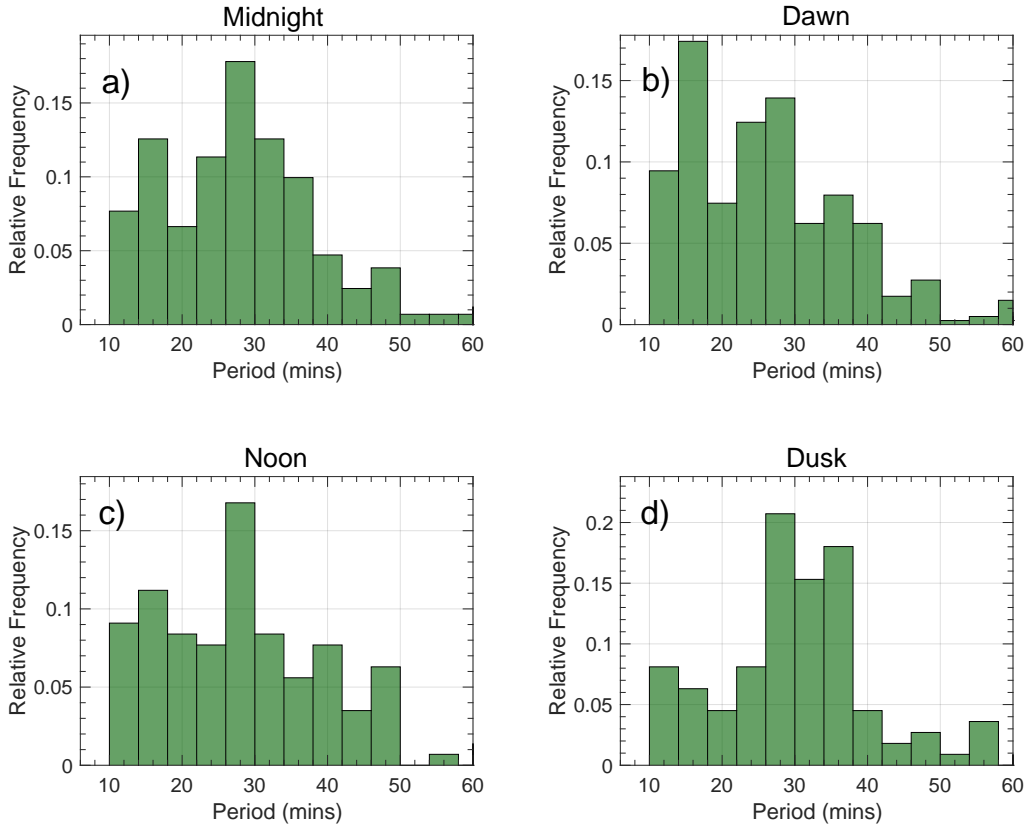


Figure 5. The distribution of periods in four local-time sectors: a) midnight, b) dawn, c) noon and d) dusk. We show only the field-transverse events, and have normalized each histogram for consistent comparisons of relative frequency. Clear skews are evident in dusk and dawn about the dominant 30 min period at noon and midnight, with dusk periods shifted to <30 min and dawn shifted to >30 min.

4 Discussion

A wealth of information is contained in the survey results, a full analysis of which is beyond the scope of this study. We will focus our discussion on the most informative consequences for large-scale dynamics of the magnetosphere.

The most striking feature of the results is the distribution of events shown in Fig. 3. For example, the magnetotail appears to have significantly different spectral properties to the dayside, and there is some evidence of a dawn-dusk asymmetry. This is consistent with expectations for the periods of SAWs excited on magnetic field lines in these local-time sectors. A persistent systematic asymmetry in magnetic field has been observed in the magnetotail, with flux tubes less stretched at dusk than at dawn (Kivelson & Khu-

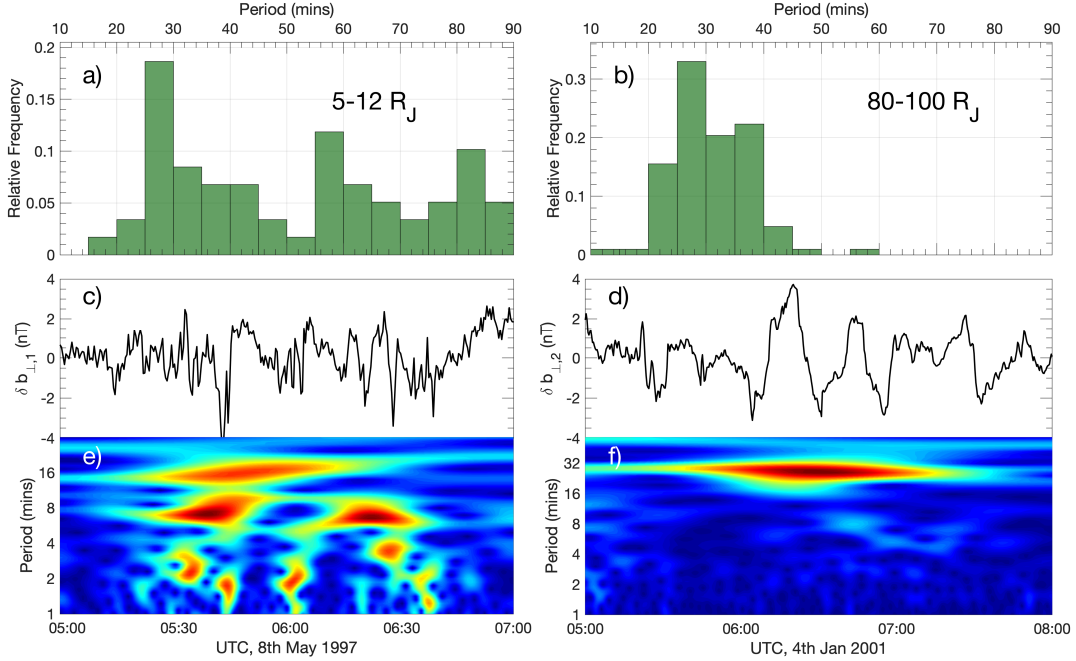


Figure 6. Case study comparing ULF waves a/c/e) near the plasma torus around Io’s orbit, and b/d/f) the vicinity of the magnetopause in the noon local-time sector; a) and b) show the distributions of periods in this regions; c) and d) show the time series of MFA residual perturbations representative of events in these regions, obtained using a 100 min sliding window; and e) and f) show the wavelet transforms of c) and d), respectively.

333 rana, 2002; K. Khurana et al., 2004). This means that the plasma sheet is thicker at dusk
 334 and thinner at dawn. SAWs at Jupiter spend the majority of their bounce-period trans-
 335 siting the dense plasma sheet, and so a systematic asymmetry in plasma-sheet thickness
 336 should correspond to an asymmetry in SAW periods. The distributions in the midnight
 337 and noon local-time sectors are similar, consistent with compressional ULF waves ex-
 338 cited on the dayside being advected around the dusk flank to the nightside. However,
 339 this does not rule out other driving mechanisms common to the midnight and noon sec-
 340 tors, or some other method of globally generating broadband spectrum ULF waves. Con-
 341 versely, on the dayside there is a clear radial trend, where bandpower of the average event
 342 in the inner magnetosphere ($<10 R_J$) is several orders of magnitude greater than in the
 343 outer magnetosphere ($>40 R_J$). Two interpretations are available: first, energy density
 344 is enhanced closer to the planet due to a focusing effect, whereby inbound MHD waves
 345 collect in the inner magnetosphere; second, separate driving mechanisms exist in the in-

346 ner magnetosphere with a much larger energy-density than drivers in the outer magne-
 347 tosphere. The most likely causes of these systematic differences can be considered us-
 348 ing analogues in the terrestrial magnetosphere for comparison.

349 **4.1 Driving mechanisms external to the magnetosphere**

ULF compressional waves in planetary magnetospheres can be externally driven by frequent perturbations on the magnetopause, some of which can be of considerable amplitude (Kepko, 2003; Zhang et al., 2010). The magnetopause is often perturbed by the solar wind, both coherently on a global scale such as during interplanetary shocks, and also locally by small-scale dynamic-pressure fluctuations. A measure of magnetospheric compressibility was derived by Glassmeier et al. (2004), expressed as

$$\kappa = \frac{1}{R_{MP}} \frac{dR_{MP}}{dP_{Dyn}}, \quad (3)$$

350 where R_{MP} is the magnetopause stand-off distance at the subsolar point as calculated
 351 using the Chapman-Ferraro approximation, and P_{Dyn} is the solar wind dynamic pres-
 352 sure. At Jupiter κ is much larger than for the other magnetospheres in the solar system,
 353 and so the magnetopause can be compressed by tens of jovian radii due to a relatively
 354 small change in the dynamic pressure of the solar wind. This enhanced susceptibility to
 355 compression is mostly due to the plasma pressure contribution from iogenic plasma (Went
 356 et al., 2011), and the presence of a ‘cushion region’ close to the magnetopause, charac-
 357 terised by plasma-depletion and more dipolar field lines (K. Khurana et al., 2004). Kelvin-
 358 Helmholtz instabilities (KHIs) also grow on the magnetopause and have been shown to
 359 introduce ULF waves into the terrestrial magnetosphere (Hasegawa et al., 2004). Mod-
 360 elling of the magnetopause at Jupiter has revealed an enhanced KHI region close to the
 361 equator, due to the presence of the equatorial plasma sheet (Masters, 2017). KHI-driven
 362 ULF waves are therefore preferentially launched into the plasma sheet. The density gra-
 363 dients at the northern and southern boundaries of the plasma sheet cause partial reflec-
 364 tion of the waves, such that the plasma sheet acts as a waveguide. This means that com-
 365 pressional ULF waves become trapped in the region where MHD mode-coupling is strongest,
 366 and so transfer to energy to the Alfvén mode in the resonance region (leading to SAWs)
 367 is likely to be more efficient than at Earth. This is potentially of great importance to
 368 an understanding of wave-wave and wave-particle interactions in the plasma sheet: (Saur,
 369 2004) suggested that the the long-standing question of why the plasma sheet temper-
 370 ature increases with distance from Jupiter may be due to an Alfvénic turbulent cascade

371 leading to heating in the plasma sheet in the middle magnetosphere; more recently, (Saur
 372 et al., 2018) suggested that the main mode of damping due to wave-particle interactions
 373 beyond $\sim 30 R_J$ is the ion-cyclotron mode, facilitated by such an Alfvénic cascade. A
 374 constant supply of large spatial-scale perturbations such as ULF waves could ensure that
 375 such a cascade is always active, and SAWs could present a method of further confining
 376 Alfvén wave energy in a relatively small region for a long times, allowing waves to break
 377 up into smaller scales and enhance this dissipation effect.

378 Constant perturbations of the magnetopause injecting broadband ULF waves into
 379 the magnetosphere is consistent with the frequent ULF activity in the outer magneto-
 380 sphere on the dayside and dusk-flank sectors (see Fig. 3c). However, if it can be assumed
 381 that this activity is the result of SAWs, a constant supply of energy from the magnetopause
 382 should permit the amplitude of SAWs to increase over time, such that the amplitude of
 383 SAWs on field lines closest to the magnetopause is greater than SAWs on field lines far-
 384 ther from the boundary. Instead, the data suggest the converse: the lowest ULF-power
 385 is found in the most ULF-active regions. This could represent large variability of the mag-
 386 netic field topology in the resonance region over long timescales. Large-amplitude SAWs
 387 require an accumulation of energy in a region where there is persistent fast-mode energy
 388 available and the MHD modes are consistently coupled by strong inhomogeneity. Any
 389 SAWs in the outer magnetosphere during a large compression of the magnetopause would
 390 be disordered and dissipated, before sufficient time has elapsed to build up large-amplitude
 391 Alfvén waves.

392 Resonant absorption occurs only at harmonics of the natural frequency of the lo-
 393 cal magnetic field line, and so a small portion of the broadband wave-energy is converted
 394 to the Alfvén mode (Glassmeier et al., 1999). Remaining wave energy is free to prop-
 395 agate to the middle magnetosphere. The waves may propagate as far as the inner mag-
 396 netosphere, where local conditions are more stable and so large-amplitude SAWs can be
 397 established. The efficiency of this radial transport of ULF energy is enhanced by the pres-
 398 ence of the plasma-sheet waveguide. Assuming that the thickness of the plasma sheet
 399 can be considered small compared to the length scales of the magnetosphere, the wave-
 400 energy-density should scale with the inverse square of the radius from the planet. Fit-
 401 ting the radial dependence of bandpower of the events identified in the survey with a power
 402 law yields an exponent of the radius of -2.18 ± 0.16 for the field-transverse components
 403 and -1.53 ± 0.21 for the field-parallel components (see Fig.3 in Supplementary Materi-

404 als). This indicates that the enhanced Alfvénic ULF power in the inner magnetosphere
 405 is consistent with inbound energy being focused into a smaller volume. The \sim -1.5 ex-
 406 ponent for the field-parallel component suggests that less energy penetrates into the in-
 407 ner magnetosphere, consistent with the mechanism of resonant absorption into the Alfvén
 408 mode, which should continue to occur during transit of the waves, as long as the reso-
 409 nance conditions are met.

410 If the majority of power is driven at the magnetopause then this suggests that ULF
 411 waves have a long lifetime in the magnetosphere and can transit the enormous distance
 412 between the magnetopause and the plasma torus at Io’s orbit – in stark contrast with
 413 the terrestrial magnetosphere, where ULF waves have been observed to dissipate in tens
 414 of min (Wang et al., 2015). We can compare this to an estimate of how far fast-mode
 415 waves could penetrate into the magnetosphere over a Jovian rotation by assuming con-
 416 servative ranges in the Alfvén and sound speed in the plasma sheet of 100-300 km/s (Bagenal
 417 et al., 2017; Kivelson, 2016). Using the expression for magnetosonic speed for oblique
 418 propagation $c_{ms} = \sqrt{c_s^2 + v_A^2}$, where c_s is the plasma sound speed, we obtain a fast-
 419 mode speed of \sim 140-420 km/s. For a nominal magnetopause standoff position of $75 R_J$
 420 and assuming the waves are moving radially in the plasma sheet waveguide, this gives
 421 a transit time of 3.5-10 hours, between roughly a third and one whole Jovian rotation.
 422 This suggests that while moving radially through the system, the waves may also be car-
 423 ried through all local times – though this is something of an overestimate, due to sub-
 424 corotation of the plasma sheet in the middle and outer magnetosphere. Nevertheless, it
 425 is feasible that at least occasionally, the fast-mode ULF waves are convected through all
 426 local times; assuming a near-constant supply of such waves from the magnetopause or
 427 other processes, the plasma sheet could be considered to contain a bath of ULF MHD
 428 wave energy at all radii and local times.

429 Where this energy collects is a prime question to investigate: the rapid radial drop-
 430 off in bandpower in the survey results suggests the energy collects in a localized resonator
 431 in the inner magnetosphere. Distinguishing a system-wide transport of energy and sep-
 432 arate resonant cavities and drivers in the inner magnetosphere requires a detailed inspec-
 433 tion of the local environment, specifically the plasma tori around Io and Europa.

4.2 Driving mechanisms in the plasma tori

Since Pioneer 10 and Voyager 1 passed through the plasma torus around Io's orbit in the 1970s, strong Alfvénic activity has been observed inside the torus (e.g. Walker and Kivelson (1981)). Bagenal (1983) demonstrated that the magnetic perturbation produced in Io's wake results in a system of SAWs that propagate azimuthally around the torus. Like the equatorial plasma sheet, the northern and southern edges of the torus have a sharp plasma-density gradient and so the torus acts a waveguide, trapping wave energy, such that the torus can sustain eigenoscillations. This 'Io Alfvén resonator' produces Alfvén energy a thousand times greater than contained in a typical ULF (Pc5) wave in the terrestrial magnetosphere (Greenwald & Walker, 1980; Goertz, 1980), and so makes a significant contribution to the total ULF activity in the magnetosphere. Glassmeier et al. (1989) showed evidence for decoupled transverse and compressional MHD waves in the torus, possibly indicating that the source is the Io-plasma interaction. They also produced estimates for the power produced by the Alfvén waves generated by the Io-plasma interactions, which are energetically consistent with decoupled toroidal (field-twisting) eigenmodes of the magnetic field lines and poloidal (radial breathing) eigenmodes of the whole torus. However, the interaction is unlikely to produce spectral signatures of large azimuthal spatial scales (small azimuthal wavenumbers), and so whether the interaction is responsible for coherent resonances of the whole torus is uncertain. Given that wave energy from externally-driven sources may collect in the inner magnetosphere, it is also possible that the torus resonantly couples to inbound compressional waves, effectively coupling perturbations on the magnetopause to eigenoscillations inside the torus.

Another possible driving mechanism is large-scale flux-tube interchange motion close to the torus. The radial diffusion of the torus plasma out into the equatorial plasma sheet is driven by the centrifugal-force differential across adjacent flux tubes (Bagenal & Delamere, 2011b). The rapid decrease in centrifugal potential of the torus plasma with radial distance from the planet provides free energy for the instability, whereby mass-loaded flux tubes are transported outwards and replaced by inward-travelling mass-depleted flux tubes. As the process is unlikely to occur at a constant rate, a heterogeneous environment is created sporadically in the torus where regions of cold, dense plasma are adjacent to regions of hot, diffuse plasma. The interactions between these regions may result in nonlinear wave-particle interactions that provide free energy for coherent eigenoscillations of the torus (Thorne et al., 1997; Kivelson et al., 1997).

4.3 ULF waves in the magnetotail

The ULF events in the tail plasma-sheet typically have spectral properties significantly different from those in the rest of the magnetosphere. The difference is evident when contrasting Fig. 3c) and d): while the majority of events contain a superposition of multiple significant periods, waves in the magnetotail from post-dusk to pre-dawn predominantly only contain one significant period. However, the same arguments regarding transport of the waves should apply, as the tail plasma-sheet should also act as a waveguide for MHD waves. Analysis of magnetometer data from both Voyager spacecraft showed significant ULF power close to the magnetic equator in the magnetotails of the outer planets, and very little in the lobes between the magnetopause and the plasma-sheet boundary-layer (K. K. Khurana et al., 1992). However, it cannot be assumed that SAWs can explain the main population of magnetotail events. Not all of the field lines are closed in the far-tail region, and the Alfvén bounce-time is too long to provide a strong coupling to the planet’s ionosphere. It is likely that a different mechanism is responsible for the tail events.

The bandpower of events in the pre-dawn sector are of systematically greater power than those post-dusk. The statistical reconnection X-line in the nightside decreases in radial distance from Jupiter moving from dusk to dawn. Cowley et al. (2003) discussed the relative contribution of Dungey-type and Vasyliunas-type (centrifugally-driven) reconnection and posited that Dungey-type is expected to be dominant dawn-side of midnight and Vasyliunas is dominant dusk-side. The clear asymmetry in power pre- and post-midnight in Fig. 3b) may be evidence of different dominant reconnection mechanisms. A lower wave power at dusk sector is consistent with mass-loaded flux-tubes undergoing reconnection ‘drizzle’ as suggested by Delamere and Bagenal (2010), wherein reconnection occurs in more frequent, more localized events. ULF waves can be produced by the resultant plasmoid formation, return plasma flow sunward, and corresponding dipolarization of the planetary magnetic field. Similar ULF wave production has been observed during magnetic substorms in the terrestrial magnetosphere (e.g. Mishin et al. (2002); Volwerk et al. (2005); Liang et al. (2009)). Vogt et al. (2014) found the mean plasmoid duration to be 6.8 min, but the distribution spanned ~ 5 -15 min, consistent with the lower end of the ULF distribution throughout the magnetosphere. They also observed the ‘chain’ reconnection bursts observed at Earth, Saturn and Mercury; over half the plasmoids they studied occurred within 90 min of a subsequent reconnection signature. This

500 suggests that though the reconnection-mechanism probably differs at Jupiter, return flows
501 and dipolarizations of the field result nevertheless, and so reconnection in the magne-
502 totail is probably a source of quasi-periodic ULF power.

503 **4.4 Redistribution of energy in the magnetosphere**

504 The foremost notable characteristic of magnetospheric ULF waves is their ability
505 to redistribute energy on a global scale. The structures and processes involved in the pro-
506 duction of ULF waves on which we have speculated are presented in Fig. 7, highlight-
507 ing the connection between compressional ULF waves and SAWs, as well as the differ-
508 ent hypothesised resonant cavities. The key element facilitating a connection between
509 these processes are SAWs, which act as energy-storage channels, trapping energy from
510 perturbations in localized regions on timescales longer than the lifetime of the initial per-
511 turbation.

512 The relative proportion of ULF wave energy that is transferred to SAWs, and the
513 relative proportion of the global energy budget that is contributed by ULF waves, are
514 both important for developing a better understanding of global dynamics – and which
515 until now have been impossible to estimate with limited data. Rae et al. (2007) estimated
516 that the proportion of SAW energy dissipated by joule heating and injected into the into
517 the Earth’s ionosphere could be as high as 30% during large substorms. While the ap-
518 plicability of the concept of substorms at Jupiter remains unclear, the findings of this
519 study indicate that during times of significant perturbations to the magnetospheric con-
520 figuration, SAWs may be a viable channel for transferring a large amount of energy from
521 the solar wind to disparate parts of the magnetosphere and into the ionosphere.

522 The importance of wave-particle interactions is paramount in the further study of
523 ULF waves and their relation to these dynamics. ULF wave-particle interactions have
524 been studied extensively in the terrestrial magnetosphere (Watt et al., 2011; Jonathan
525 Rae et al., 2018), and have been shown to modulate precipitation of energetic electrons
526 into the ionosphere and growth-rates of kinetic-scale waves, both of which have impor-
527 tant implications for the highly variable aurora at Jupiter. The dissipation of SAWs has
528 been shown to consist of a complex interplay between properties of the wave, ambient
529 plasma and the ionosphere; joule heating in the ionosphere, landau damping and elec-
530 tron trapping in quasi-static field-parallel electric fields have all been shown to contribute
531 to damping (Rankin et al., 2007; Jonathan Rae et al., 2018). ULF energy is also known

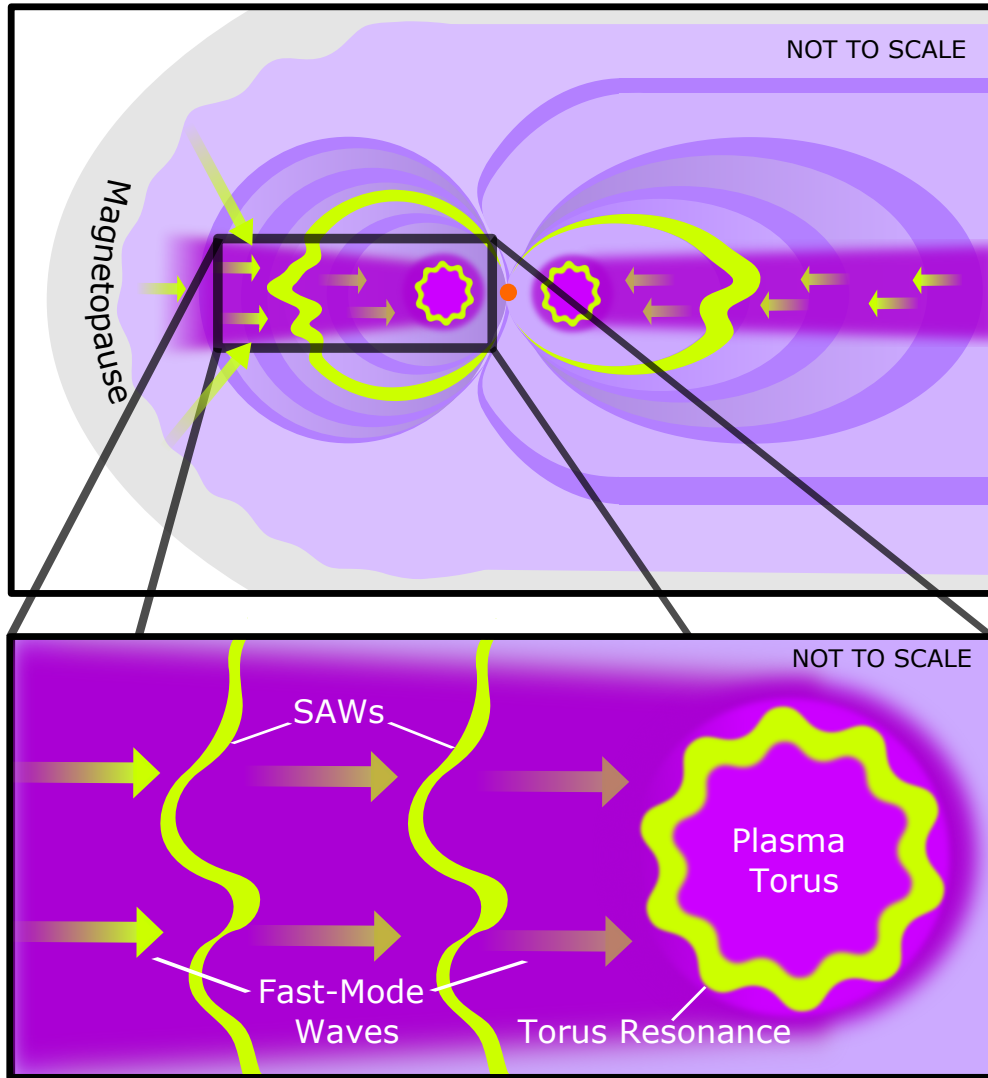


Figure 7. A cartoon of the chain of processes responsible for ULF wave generation in the magnetosphere. The magnetospheric cavity is shown in light purple, and magnetic field lines are represented in dark purple. Perturbations on the magnetopause create compressional fast-mode waves (green arrows) that propagate planetward, confined to the plasma-sheet waveguide (pink). SAWs are generated locally where the inbound compressional waves match the field line eigenperiods (distorted green field lines). Remaining propagating wave energy collects in the inner magnetosphere where it is resonantly absorbed by the Io plasma torus. Reconnection processes in the magnetotail create a separate population of monochromatic SAWs, also confined to the equatorial waveguide.

532 to be redistributed around the flanks of the terrestrial magnetosphere by a magnetotail
 533 waveguide (see Wang et al. (2015) and references therein), whereby compressional ULF
 534 waves are advected anti-sunward while reflecting between the magnetopause and an in-
 535 ner turning point closer to the planet.

536 The outer planets have multiple energy crises within their magnetosphere-ionosphere-
 537 thermosphere systems, such as the heating of the plasma sheet with increasing radial dis-
 538 tance from the planet (see e.g. Bagenal and Delamere (2011b)). In the aftermath of JUNO’s
 539 first traversals of Jupiter’s polar regions, the established paradigm of quasi-static cur-
 540 rent systems transporting energy and angular momentum from the planet out into the
 541 mass-loaded magnetosphere cannot provide a full explanation of global dynamics. The
 542 broadband bidirectional electron beams frequently observed in regions where strong FACs
 543 are expected suggest that stochastic acceleration plays a large role in particle heating
 544 and auroral precipitation (e.g. Clark et al. (2017); Connerney et al. (2017); B. H. Mauk
 545 et al. (2017a, 2018)). Non-steady processes have also been suggested elsewhere in the
 546 magnetosphere: the plasma sheet is known to exhibit MHD turbulence that may be re-
 547 sponsible for heating of the middle- and outer-magnetospheric plasma (Saur et al., 2002;
 548 Saur, 2004). A recent study by Saur et al. (2018) highlighted the importance of Alfvénic
 549 turbulent-cascades and dissipation in the magnetosphere as a source of particle accel-
 550 eration, specifically that the dominant mode of dissipation varies in different regions of
 551 the magnetosphere. Given the ubiquitous presence of QPOs, ULF waves are very likely
 552 to play a role in the modulation of wave-growth and scattering processes, and direct en-
 553 ergization of ambient plasma.

554 **4.5 Summary**

555 Transplanting existing ULF wave theory to the jovian magnetosphere remains non-
 556 trivial and ongoing, but the heritage survey of magnetometer data we have presented
 557 here provides the first look at the systematic global distribution of waves in the equa-
 558 torial plane. The results demonstrate that ULF waves occur most often in the outer mag-
 559 netosphere on the dayside and along the dusk flank, but ULF wave energy is concentrated
 560 in the inner magnetosphere. We speculated that this may be due to a combination of
 561 different resonant cavities, one in the equatorial plasma sheet and another in the plasma
 562 torus around Io’s orbit, though this hypothesis cannot be verified using these data alone.
 563 Spectral properties of QPOs previously observed throughout the system are consistent

564 with the ULF spectrum obtained from the survey: a distribution spanning 5 - 60 min,
 565 dominated by 15, 30 and 40 min. The population is well described by a large popula-
 566 tion of transhemispheric SAWs confined to the plasma sheet. The magnetotail plasma-
 567 sheet appears to host a separate population of quasi-monochromatic ULF waves, which
 568 we interpreted as evidence of a different driving mechanism dominated by reconnection
 569 and dipolarization of the magnetic field. ULF waves are a key element in understand-
 570 ing both the global processes which redistribute energy through the magnetosphere, and
 571 resonant cavities that act as localized reservoirs of energy. Answering questions of how
 572 these cavities contribute to particle energization, stochastic acceleration and energy/momentum
 573 transport in the magnetosphere will require a detailed analysis of ULF wave-modes and
 574 the wave-particle interactions in which they participate.

575 Acknowledgments

576 Harry Manners is supported by a Royal Society PhD Studentship. Adam Masters is sup-
 577 ported by a Royal Society University Research Fellowship. Magnetometer data from all
 578 of the spacecraft data used in this study can be obtained from the NASA Planetary Data
 579 System (<https://pds.nasa.gov>). Data required to reproduce the results shown is stored
 580 in the Zenodo repository at DOI: 10.5281/zenodo.3898560. Please direct correspondence
 581 to Harry Manners (h.manners17@imperial.ac.uk).

582 DOI: 10.5281/zenodo.3898560

583 References

- 584 Achilleos, N., André, N., Blanco-Cano, X., Brandt, P. C., Delamere, P. A., &
 585 Winglee, R. (2015). 1. Transport of Mass, Momentum and Energy in
 586 Planetary Magnetodisc Regions. *Space Sci. Rev.*, *187*(1-4), 229–299. doi:
 587 10.1007/s11214-014-0086-y
- 588 Acuna, M. H., & Ness, N. F. (1980). The Magnetic Field of Saturn: Pioneer 11 Ob-
 589 servations. *Science (80-.)*, *207*(4429), 444–446. doi: 10.1126/science.207.4429
 590 .444
- 591 Allegrini, F., Bagenal, F., Bolton, S., Connerney, J., Clark, G., Ebert, R. W., ...
 592 Zink, J. L. (2017). Electron beams and loss cones in the auroral regions of
 593 Jupiter. *Geophys. Res. Lett.*, *44*(14), 7131–7139. doi: 10.1002/2017GL073180
- 594 Anagnostopoulos, G., Aggelis, A., Karanikola, I., & Marhavilas, P. (2001). Ener-

- 595 getic ion ($>\sim 50\text{keV}$) and electron ($>\sim 40\text{keV}$) bursts observed by Ulysses near
596 Jupiter. *Adv. Sp. Res.*, 28(6), 903–908. doi: 10.1016/S0273-1177(01)00514-2
- 597 Arkhypov, O. V., & Rucker, H. O. (2006). Ultra low frequencies phenomena in Jo-
598 vian decametric radio emission. *Astron. Astrophys.*, 452(1), 347–350. doi: 10
599 .1051/0004-6361:20054334
- 600 Bagenal, F. (1983). Alfvén wave propagation in the Io plasma torus. *J. Geo-
601 phys. Res. Sp. Phys.*, 88(A4), 3013–3025. Retrieved from [http://dx.doi.org/
602 10.1029/JA088iA04p03013](http://dx.doi.org/10.1029/JA088iA04p03013) doi: 10.1029/JA088iA04p03013
- 603 Bagenal, F., Adriani, A., Allegrini, F., Bolton, S. J., Bonfond, B., Bunce, E. J., ...
604 Zarka, P. (2017). Magnetospheric Science Objectives of the Juno Mission.
605 *Space Sci. Rev.*, 213(1-4), 219–287. doi: 10.1007/s11214-014-0036-8
- 606 Bagenal, F., & Delamere, P. A. (2011a). Flow of mass and energy in the magneto-
607 spheres of Jupiter and Saturn. *J. Geophys. Res. Sp. Phys.*, 116(A5), 1–17. doi:
608 10.1029/2010JA016294
- 609 Bagenal, F., & Delamere, P. A. (2011b). Flow of mass and energy in the magneto-
610 spheres of Jupiter and Saturn. *J. Geophys. Res. Sp. Phys.*, 116(5), 1–17. doi:
611 10.1029/2010JA016294
- 612 Bagenal, F., Wilson, R. J., Siler, S., Paterson, W. R., & Kurth, W. S. (2016). Sur-
613 vey of Galileo plasma observations in Jupiter’s plasma sheet. *J. Geophys. Res.
614 Planets*, 121(5), 871–894. doi: 10.1002/2016JE005009
- 615 Barbosa, D. D., Gurnett, D. A., Kurth, W. S., & Scarf, F. L. (1979). Structure
616 and properties of Jupiter’s magnetoplasma disc. *Geophys. Res. Lett.*, 6(10),
617 785–788. doi: 10.1029/GL006i010p00785
- 618 Bolton, S. J., Janssen, M., Thorne, R., Levin, S., Klein, M., Gulkis, S., ... West,
619 R. (2002). Ultra-relativistic electrons in Jupiter’s radiation belts. *Nature*,
620 415(6875), 987–991. doi: 10.1038/415987a
- 621 Chen, L., & Hasegawa, A. (1974). A theory of long-period magnetic pulsations: 1.
622 Steady state excitation of field line resonance. *J. Geophys. Res.*, 79(7), 1024–
623 1032. doi: 10.1029/JA079i007p01024
- 624 Clark, G., Mauk, B. H., Haggerty, D., Paranicas, C., Kollmann, P., Rymer, A., ...
625 Valek, P. (2017). Energetic particle signatures of magnetic field-aligned poten-
626 tials over Jupiter’s polar regions. *Geophys. Res. Lett.*, 44(17), 8703–8711. doi:
627 10.1002/2017GL074366

- 628 Connerney, J. E., Adriani, A., Allegrini, F., Bagenal, F., Bolton, S. J., Bonfond,
629 B., . . . Waite, J. (2017). Jupiter’s magnetosphere and aurorae observed by
630 the Juno spacecraft during its first polar orbits. *Science (80-.)*, *356*(6340),
631 826–832. doi: 10.1126/science.aam5928
- 632 Cowley, S. W. H., Bunce, E. J., Stallard, T. S., & Miller, S. (2003). Jupiter’s polar
633 ionospheric flows: Theoretical interpretation. *Geophys. Res. Lett.*, *30*(5), n/a–
634 n/a. doi: 10.1029/2002GL016030
- 635 Delamere, P. A. (2016). A Review of the Low-Frequency Waves in the Gi-
636 ant Magnetospheres. *Low-Frequency Waves Sp. Plasmas*, 365–378. doi:
637 10.1002/9781119055006.ch21
- 638 Delamere, P. A., & Bagenal, F. (2010). Solar wind interaction with Jupiter’s mag-
639 netosphere. *J. Geophys. Res. Sp. Phys.*, *115*(A10), n/a–n/a. doi: 10.1029/
640 2010JA015347
- 641 Dunn, W. R., Branduardi-Raymont, G., Ray, L. C., Jackman, C. M., Kraft, R. P.,
642 Elsner, R. F., . . . Coates, A. J. (2017). The independent pulsations of Jupiter’s
643 northern and southern X-ray auroras. *Nat. Astron.*, *1*(11), 758–764. doi:
644 10.1038/s41550-017-0262-6
- 645 Ebert, R. W., Allegrini, F., Bagenal, F., Bolton, S. J., Connerney, J. E., Clark, G.,
646 . . . Wilson, R. J. (2017). Spatial Distribution and Properties of 0.1100keV
647 Electrons in Jupiter’s Polar Auroral Region. *Geophys. Res. Lett.*, *44*(18),
648 9199–9207. doi: 10.1002/2017GL075106
- 649 Frank, L. A., Ackerson, K. L., Lee, J. A., English, M. R., & Pickett, G. L. (1992).
650 The plasma instrumentation for the Galileo Mission. *Space Sci. Rev.*, *60*(1-4),
651 283–304. doi: 10.1007/BF00216858
- 652 Gershman, D. J., Connerney, J. E. P., Kotsiaros, S., DiBraccio, G. A., Martos,
653 Y. M., Viñas, A. F., . . . Bolton, S. J. (2019). Alfvénic Fluctuations Associated
654 With Jupiter’s Auroral Emissions. *Geophys. Res. Lett.*, *46*(13), 7157–7165. doi:
655 10.1029/2019GL082951
- 656 Gladstone, G. R., Waite, J. H., Grodent, D., Lewis, W. S., Crary, F. J., Eisner,
657 R. F., . . . Cravens, T. E. (2002). A pulsating auroral X-ray hot spot on
658 Jupiter. *Nature*, *415*(6875), 1000–1003. doi: 10.1038/4151000a
- 659 Glassmeier, K. H., Klimushkin, D., Othmer, C., & Mager, P. (2004). ULF waves at
660 Mercury: Earth, the giants, and their little brother compared. *Adv. Sp. Res.*,

- 661 33(11), 1875–1883. doi: 10.1016/j.asr.2003.04.047
- 662 Glassmeier, K.-H., Ness, N. F., Acuña, M. H., & Neubauer, F. M. (1989). Standing
663 hydromagnetic waves in the Io plasma torus: Voyager 1 observations. *J. Geo-*
664 *phys. Res.*, 94(A11), 15063. doi: 10.1029/JA094iA11p15063
- 665 Glassmeier, K. H., Othmer, C., Cramm, R., Stellmacher, M., & Engebretson, M.
666 (1999). Magnetospheric field line resonance: A comparative planetology ap-
667 proach. *Surv. Geophys.*, 20(1), 61–109. doi: 10.1023/A:1006659717963
- 668 Goertz, C. (1980). Io’s interaction with the plasma torus. *J. Geophys. Res.*, 85(A6),
669 2949. doi: 10.1029/JA085iA06p02949
- 670 Greenwald, R. A., & Walker, A. D. M. (1980). Energetics of long period resonant
671 hydromagnetic waves. *Geophys. Res. Lett.*, 7(10), 745–748. doi: 10.1029/
672 GL007i010p00745
- 673 Hasegawa, H., Fujimoto, M., Phan, T.-D., Rème, H., Balogh, A., Dunlop, M. W., ...
674 TanDokoro, R. (2004). Transport of solar wind into Earth’s magnetosphere
675 through rolled-up KelvinHelmholtz vortices. *Nature*, 430(7001), 755–758. doi:
676 10.1038/nature02799
- 677 Hospodarsky, G. B., Kurth, W. S., Cecconi, B., Gurnett, D. A., Kaiser, M. L.,
678 Desch, M. D., & Zarka, P. (2004). Simultaneous observations of Jovian quasi-
679 periodic radio emissions by the Galileo and Cassini spacecraft. *J. Geophys.*
680 *Res. Sp. Phys.*, 109(A9), 1–13. doi: 10.1029/2003JA010263
- 681 Jonathan Rae, I., Murphy, K. R., Watt, C. E. J., Halford, A. J., Mann, I. R., Ozeke,
682 L. G., ... Singer, H. J. (2018). The Role of Localized Compressional Ultra-low
683 Frequency Waves in Energetic Electron Precipitation. *J. Geophys. Res. Sp.*
684 *Phys.*, 123(3), 1900–1914. doi: 10.1002/2017JA024674
- 685 Joy, S. P., Kivelson, M. G., Walker, R. J., Khurana, K. K., Russell, C. T., &
686 Ogino, T. (2002). Probabilistic models of the Jovian magnetopause and
687 bow shock locations. *J. Geophys. Res. Sp. Phys.*, 107(A10), 1–17. doi:
688 10.1029/2001JA009146
- 689 Karanikola, I., Athanasiou, M., Anagnostopoulos, G. C., Pavlos, G. P., & Preka-
690 Papadema, P. (2004). Quasi-periodic emissions (15- 80 min) from the poles
691 of Jupiter as a principal source of the large-scale high-latitude magnetopause
692 boundary layer of energetic particle. *Planet. Space Sci.*, 52(5-6), 543–559. doi:
693 10.1016/j.pss.2003.10.002

- 694 Kepko, L. (2003). Observations of discrete, global magnetospheric oscillations di-
 695 rectly driven by solar wind density variations. *J. Geophys. Res.*, *108*(A6),
 696 1257. doi: 10.1029/2002JA009676
- 697 Khurana, K., & Kivelson, M. (1989). Ultralow frequency MHD waves in
 698 Jupiter’s middle magnetosphere. *J. Geophys. Res.*, *94*(A5), 5241. doi:
 699 10.1029/JA094iA05p05241
- 700 Khurana, K., Kivelson, M., Vasyliunas, V., Krupp, N., Woch, J., Lagg, A., ...
 701 Kurth, W. (2004). The Configuration of Jupiter’s Magnetosphere. *Jupiter*
 702 *Planet, Satell. Magnetos.*, 593–616. doi: 10.1007/s00216-006-0600-5
- 703 Khurana, K. K., Sheng Hsien Chen, Max Hammond, C., & Kivelson, M. G. (1992).
 704 Ultralow frequency waves in the magnetotails of the Earth and the outer plan-
 705 ets. *Adv. Sp. Res.*, *12*(8), 57–63. doi: 10.1016/0273-1177(92)90377-A
- 706 Kimura, T., Cecconi, B., Zarka, P., Kasaba, Y., Tsuchiya, F., Misawa, H., &
 707 Morioka, A. (2012). Polarization and direction of arrival of Jovian quasiperi-
 708 odic bursts observed by Cassini. *J. Geophys. Res. Sp. Phys.*, *117*(11), 1–15.
 709 doi: 10.1029/2012JA017506
- 710 Kimura, T., Tsuchiya, F., Misawa, H., Morioka, A., Nozawa, H., & Fujimoto, M.
 711 (2011). Periodicity analysis of Jovian quasi-periodic radio bursts based on
 712 Lomb-Scargle periodograms. *J. Geophys. Res. Sp. Phys.*, *116*(3), 1–10. doi:
 713 10.1029/2010JA016076
- 714 Kivelson, M. G. (2016). Planetary Magnetodiscs: Some Unanswered Questions.
 715 In *The magnetodiscs and aurorae of giant planets* (pp. 5–21). New York, NY:
 716 Springer. doi: 10.1007/978-1-4939-3395-2_2
- 717 Kivelson, M. G., & Khurana, K. K. (2002). Properties of the magnetic field in the
 718 Jovian magnetotail. *J. Geophys. Res. Sp. Phys.*, *107*(A8), SMP 23–1–SMP 23–
 719 9. doi: 10.1029/2001JA000249
- 720 Kivelson, M. G., Khurana, K. K., Means, J. D., Russell, C. T., & Snare, R. C.
 721 (1992). The Galileo magnetic field investigation. *Space Sci. Rev.*, *60*(1-4),
 722 357–383. doi: 10.1007/BF00216862
- 723 Kivelson, M. G., Khurana, K. K., Russell, C. T., & Walker, R. J. (1997). Inter-
 724 mittent short-duration magnetic field anomalies in the Io torus: Evidence
 725 for plasma interchange? *Geophys. Res. Lett.*, *24*(17), 2127–2130. doi:
 726 10.1029/97GL02202

- 727 Kohlhasse, C., & Penzo, P. (1977). Voyager mission description. *Space Sci. Rev.*,
728 *21*(2), 77–101. doi: 10.1007/BF00200846
- 729 Kotsiaros, S., Connerney, J. E. P., Clark, G., Allegrini, F., Gladstone, G. R., Kurth,
730 W. S., ... Levin, S. M. (2019). Birkeland currents in Jupiter’s magneto-
731 sphere observed by the polar-orbiting Juno spacecraft. *Nat. Astron.* doi:
732 10.1038/s41550-019-0819-7
- 733 Liang, J., Liu, W. W., Donovan, E. F., & Spanswick, E. (2009). In-situ obser-
734 vation of ULF wave activities associated with substorm expansion phase
735 onset and current disruption. *Ann. Geophys.*, *27*(5), 2191–2204. doi:
736 10.5194/angeo-27-2191-2009
- 737 MacDowall, R. J., Kaiser, M. L., Desch, M. D., Farrell, W. M., Hess, R. A., & Stone,
738 R. G. (1993). Quasiperiodic Jovian Radio bursts: observations from the
739 Ulysses Radio and Plasma Wave Experiment. *Planet. Space Sci.*, *41*(11-12),
740 1059–1072. doi: 10.1016/0032-0633(93)90109-F
- 741 Manners, H., & Masters, A. (2019). First Evidence for MultipleHarmonic Stand-
742 ing Alfvén Waves in Jupiter’s Equatorial Plasma Sheet. *Geophys. Res. Lett.*,
743 2019GL083899. doi: 10.1029/2019GL083899
- 744 Manners, H., Masters, A., & Yates, J. N. (2018). Standing Alfvén Waves in Jupiter’s
745 Magnetosphere as a Source of ~10- to 60-Min Quasiperiodic Pulsations. *Geo-
746 phys. Res. Lett.*, *45*(17), 8746–8754. doi: 10.1029/2018GL078891
- 747 Masters, A. (2017). Model-Based Assessments of Magnetic Reconnection and
748 Kelvin-Helmholtz Instability at Jupiter’s Magnetopause. *J. Geophys. Res. Sp.
749 Phys.*, *122*(11), 11,154–11,174. doi: 10.1002/2017JA024736
- 750 Mauk, B., & Bagenal, F. (2013). Comparative Auroral Physics: Earth and Other
751 Planets. *Auror. Phenomenol. Magnetos. Process. Earth Other Planets*, 3–26.
752 doi: 10.1029/2011GM001192
- 753 Mauk, B. H., Haggerty, D. K., Paranicas, C., Clark, G., Kollmann, P., Rymer,
754 A. M., ... Valek, P. (2017a). Discrete and broadband electron accel-
755 eration in Jupiter’s powerful aurora. *Nature*, *549*(7670), 66–69. doi:
756 10.1038/nature23648
- 757 Mauk, B. H., Haggerty, D. K., Paranicas, C., Clark, G., Kollmann, P., Rymer,
758 A. M., ... Valek, P. (2017b). Juno observations of energetic charged par-
759 ticles over Jupiter’s polar regions: Analysis of monodirectional and bidi-

- 760 rectional electron beams. *Geophys. Res. Lett.*, *44*(10), 4410–4418. doi:
761 10.1002/2016GL072286
- 762 Mauk, B. H., Haggerty, D. K., Paranicas, C., Clark, G., Kollmann, P., Rymer,
763 A. M., ... Valek, P. (2018). Diverse Electron and Ion Acceleration Char-
764 acteristics Observed Over Jupiter’s Main Aurora. *Geophys. Res. Lett.*, *45*(3),
765 1277–1285. doi: 10.1002/2017GL076901
- 766 Mishin, E. V., Foster, J. C., Potekhin, A. P., Rich, F. J., Schlegel, K., Yumoto, K.,
767 ... Friedel, R. (2002). Global ULF disturbances during a stormtime substorm
768 on 25 September 1998. *J. Geophys. Res. Sp. Phys.*, *107*(A12), SMP 40–1–SMP
769 40–11. doi: 10.1029/2002JA009302
- 770 Nichols, J. D., Yeoman, T. K., Bunce, E. J., Chowdhury, M. N., Cowley, S. W. H., &
771 Robinson, T. R. (2017). Periodic emission within Jupiter’s main auroral oval.
772 *Geophys. Res. Lett.*. doi: 10.1002/2017GL074824
- 773 Petkaki, P., & Dougherty, M. K. (2001). ULF wave observations in Jupiter’s magne-
774 tosphere. *Adv. Sp. Res.*, *28*(6), 909–914. doi: 10.1016/S0273-1177(01)00517-8
- 775 Rae, I. J., C. E. J., Fenrich, F. R., Mann, I. R., Ozeke, L. G., & Kale, A. (2007).
776 Energy deposition in the ionosphere through a global field line resonance. *Ann.*
777 *Geophys.*, *25*(12), 2529–2539. doi: 10.5194/angeo-25-2529-2007
- 778 Rankin, R., Watt, C. E. J., & Samson, J. C. (2007). Self-consistent wave-particle
779 interactions in dispersive scale long-period field-line-resonances. *Geophys. Res.*
780 *Lett.*, *34*(23), n/a–n/a. doi: 10.1029/2007GL031317
- 781 Russell, C. T., Blanco-Cano, X., & Strangeway, R. J. (2001). Ultra-low-frequency
782 waves in the Jovian magnetosphere: Causes and consequences. *Planet. Space*
783 *Sci.*, *49*(3-4), 291–301. doi: 10.1016/S0032-0633(00)00150-1
- 784 Saur, J. (2004). Turbulent Heating of Jupiter’s Middle Magnetosphere. *Astrophys.*
785 *J.*, *602*(2), L137–L140. doi: 10.1086/382588
- 786 Saur, J., Janser, S., Schreiner, A., Clark, G., Mauk, B. H., Kollmann, P., ... Kot-
787 siaros, S. (2018). WaveParticle Interaction of Alfvén Waves in Jupiter’s Mag-
788 netosphere: Auroral and Magnetospheric Particle Acceleration. *J. Geophys.*
789 *Res. Sp. Phys.*, *123*(11), 9560–9573. doi: 10.1029/2018JA025948
- 790 Saur, J., Politano, H., Pouquet, A., & Matthaeus, W. H. (2002). Evidence for weak
791 MHD turbulence in the middle magnetosphere of Jupiter. *Astron. Astrophys.*,
792 *386*(2), 699–708. doi: 10.1051/0004-6361:20020305

- 793 Schulz, M., Blake, J., Mazuk, S. M., Balogh, A., Dougherty, M. K., Forsyth, R. J.,
 794 ... Bame, S. J. (1993). Energetic particle, plasma and magnetic field signa-
 795 tures of a poloidal pulsation in Jupiter's magnetosphere. *Planet. Space Sci.*,
 796 *41*(11-12), 967–975. doi: 10.1016/0032-0633(93)90101-7
- 797 Smith, E. J., Wenzel, K. P., & Page, D. E. (1992). Ulysses at Jupiter: An Overview
 798 of the Encounter. *Science (80-.)*, *257*(5076), 1503–1507. doi: 10.1126/science
 799 .257.5076.1503
- 800 Southwood, D., & Hughes, W. (1983). Theory of hydromagnetic waves in the mag-
 801 netosphere. *Space Sci. Rev.*, *35*(4), 301–366. doi: 10.1007/BF00169231
- 802 Southwood, D. J. (1974). Some features of field line resonances in the magneto-
 803 sphere. *Planet. Space Sci.*, *22*(3), 483–491. doi: 10.1016/0032-0633(74)90078
 804 -6
- 805 Southwood, D. J., & Kivelson, M. G. (1986). The effect of parallel inhomogeneity on
 806 magnetospheric hydromagnetic wave coupling. *J. Geophys. Res.*, *91*(A6), 6871.
 807 doi: 10.1029/JA091iA06p06871
- 808 Tamao, T. (1965). Transmission and Coupling Resonance of Hydromagnetic Distur-
 809 bances in the Non-uniform Earth's Magnetosphere. *Sci. reports Tohoku Univ.*
 810 *Ser. 5, Geophys.*, *17*(2), 43–72.
- 811 Thorne, R. M., Armstrong, T. P., Stone, S., Williams, D. J., McEntire, R. W.,
 812 Bolton, S. J., ... Kivelson, M. G. (1997). Galileo evidence for rapid inter-
 813 change transport in the Io torus. *Geophys. Res. Lett.*, *24*(17), 2131–2134. doi:
 814 10.1029/97GL01788
- 815 Torrence, C., & Compo, G. P. (1998). A Practical Guide to Wavelet Analysis. *Bull.*
 816 *Am. Meteorol. Soc.*, *79*(1), 61–78. doi: 10.1175/1520-0477(1998)079<0061:
 817 APGTWA>2.0.CO;2
- 818 Tsurutani, B. T., Southwood, D. J., Smith, E. J., & Balogh, A. (1993). A Survey
 819 of Low Frequency Waves at Jupiter: The Ulysses Encounter. *J. Geophys. Res.*,
 820 *98*(A12), 21203–21216. doi: 10.1029/93JA02586
- 821 Van Allen, J. A., Baker, D. N., Randall, B. A., & Sentman, D. D. (1974). The mag-
 822 netosphere of Jupiter as observed with Pioneer 10: 1. Instrument and principal
 823 findings. *J. Geophys. Res.*, *79*(25), 3559–3577. doi: 10.1029/JA079i025p03559
- 824 Vogt, M. F., Jackman, C. M., Slavin, J. A., Bunce, E. J., Cowley, S. W. H., Kivel-
 825 son, M. G., & Khurana, K. K. (2014). Structure and statistical properties

- 826 of plasmoids in Jupiter's magnetotail. *J. Geophys. Res. Sp. Phys.*, 119(2),
827 821–843. doi: 10.1002/2013JA019393
- 828 Volwerk, M., Zhang, T. L., Nakamura, R., Runov, A., Baumjohann, W., Glass-
829 meier, K.-H., . . . Rème, H. (2005). Plasma flow channels with ULF waves
830 observed by Cluster and Double Star. *Ann. Geophys.*, 23(8), 2929–2935. doi:
831 10.5194/angeo-23-2929-2005
- 832 Walker, R., & Kivelson, M. (1981). Multiply reflected standing Alfvén waves in the
833 IO torus: Pioneer 10 observations. *Geophys. Res. Lett.*, 8(12), 1281–1284. doi:
834 10.1029/GL008i012p01281
- 835 Wang, C., Rankin, R., & Zong, Q. (2015). Fast damping of ultralow frequency waves
836 excited by interplanetary shocks in the magnetosphere. *J. Geophys. Res. Sp.*
837 *Phys.*, 120(4), 2438–2451. doi: 10.1002/2014JA020761
- 838 Watanabe, H., Kita, H., Tao, C., Kagitani, M., Sakanoi, T., & Kasaba, Y. (2018).
839 Pulsation Characteristics of Jovian Infrared Northern Aurora Observed by
840 the Subaru IRCS with Adaptive Optics. *Geophys. Res. Lett.*, 547–554. doi:
841 10.1029/2018GL079411
- 842 Watt, C. E. J., Degeling, A. W., Rankin, R., Murphy, K. R., Rae, I. J., & Singer,
843 H. J. (2011). Ultralow-frequency modulation of whistler-mode wave growth. *J.*
844 *Geophys. Res. Sp. Phys.*, 116(A10). doi: 10.1029/2011JA016730
- 845 Went, D. R., Kivelson, M. G., Achilleos, N., Arridge, C. S., & Dougherty, M. K.
846 (2011). Outer magnetospheric structure: Jupiter and Saturn compared. *J.*
847 *Geophys. Res. Sp. Phys.*, 116(4), 1–14. doi: 10.1029/2010JA016045
- 848 Wilson, R. J., & Dougherty, M. K. (2000). Evidence provided by Galileo of ultra low
849 frequency waves within Jupiter's middle magnetosphere. *Geophys. Res. Lett.*,
850 27(6), 835–838. doi: 10.1029/1999GL006070
- 851 Wright, A. N., & Mann, I. R. (2013). Global MHD Eigenmodes of the Outer Mag-
852 netosphere. *Magnetos. ULF Waves Synth. New Dir.*, 169, 51–72. doi: 10.1029/
853 169GM06
- 854 Zhang, X. Y., Zong, Q.-G., Wang, Y. F., Zhang, H., Xie, L., Fu, S. Y., . . . Pu, Z. Y.
855 (2010). ULF waves excited by negative/positive solar wind dynamic pressure
856 impulses at geosynchronous orbit. *J. Geophys. Res. Sp. Phys.*, 115(A10),
857 n/a–n/a. doi: 10.1029/2009JA015016

Figure.

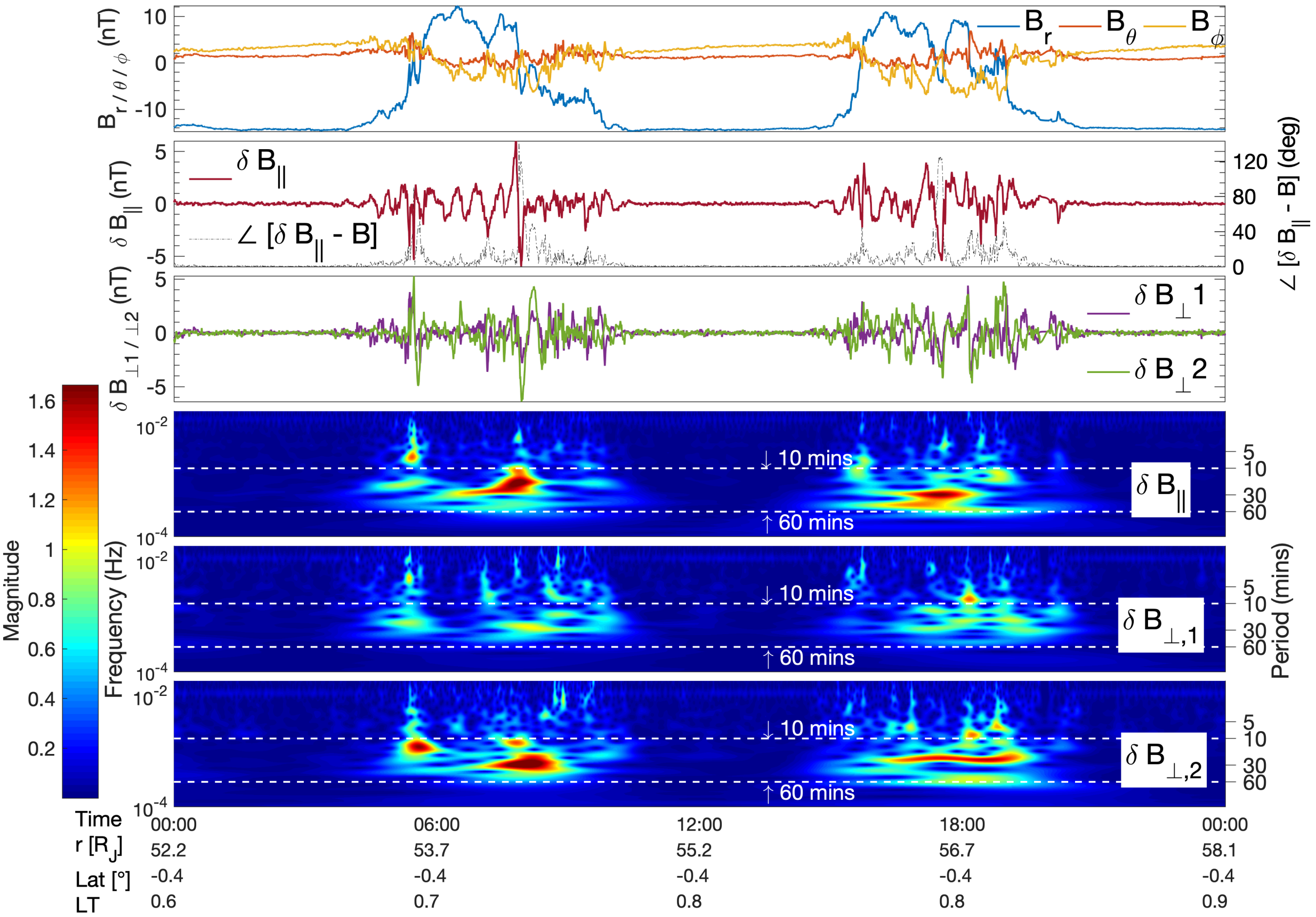


Figure.

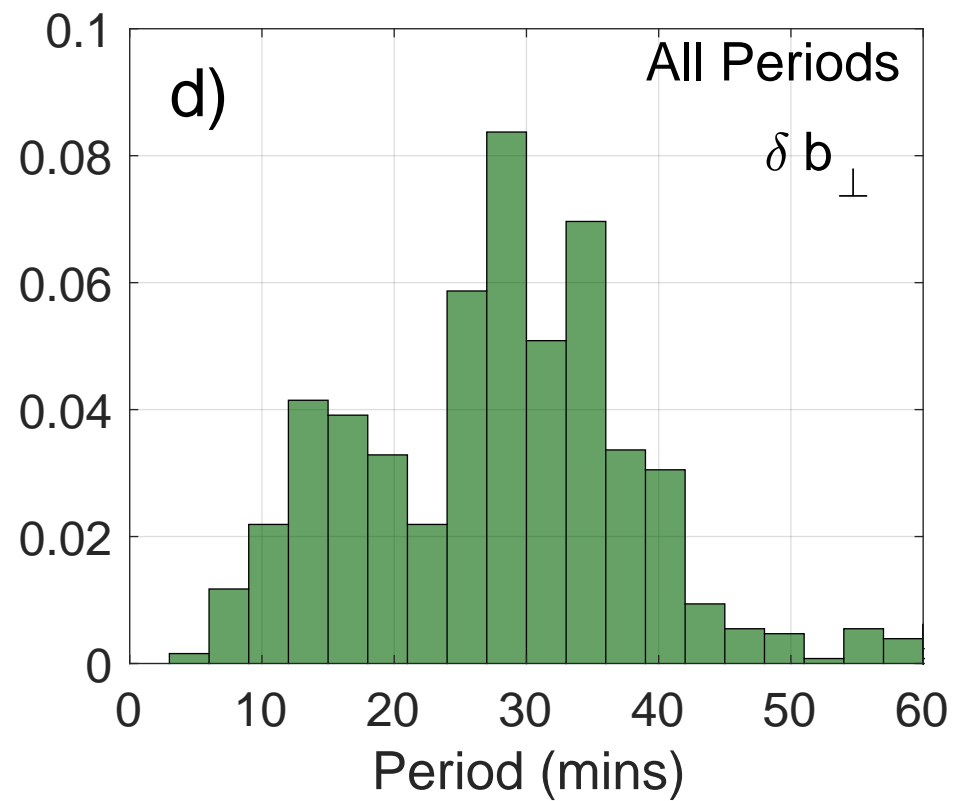
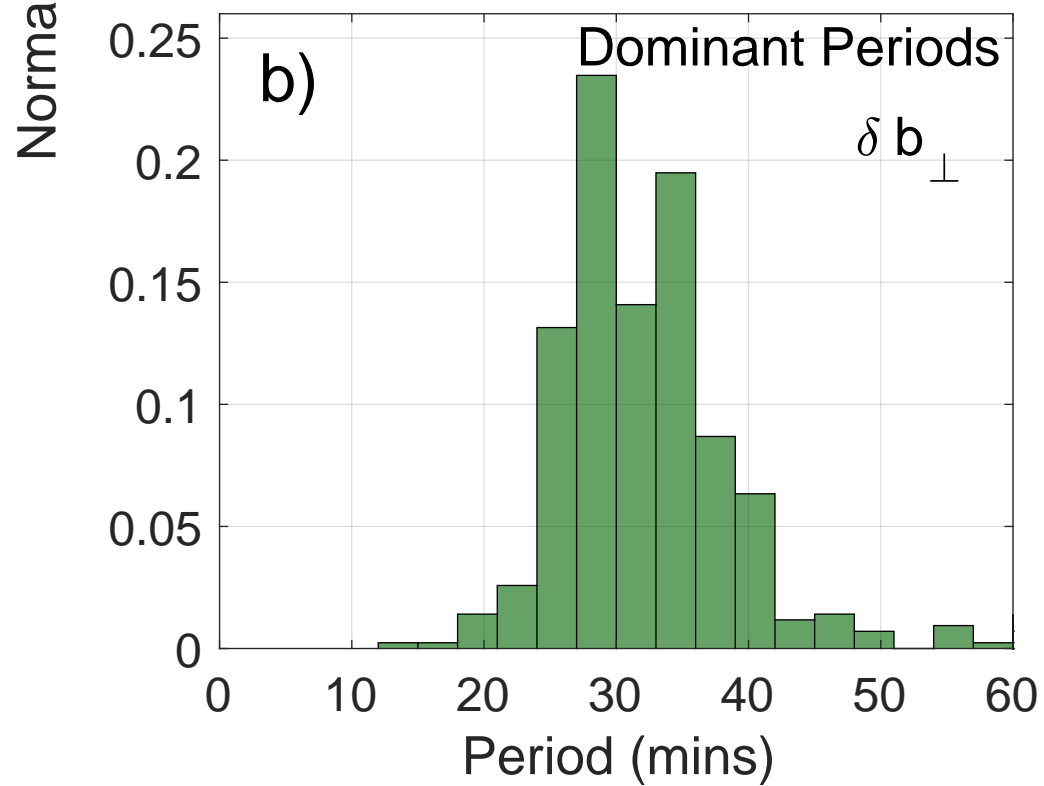
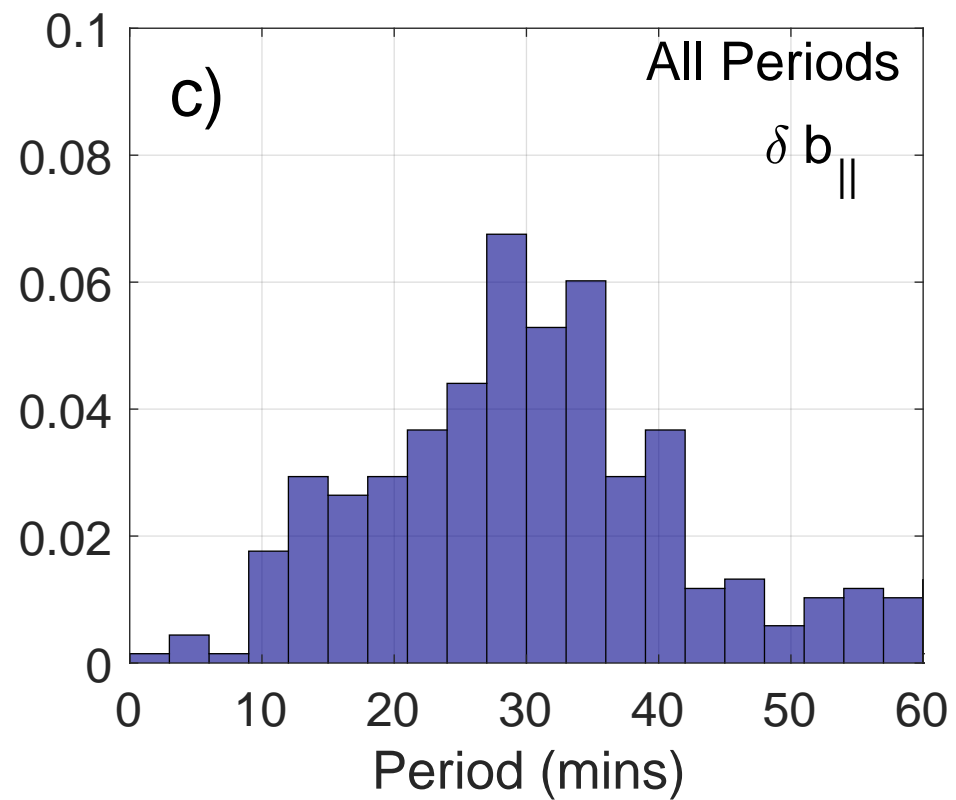
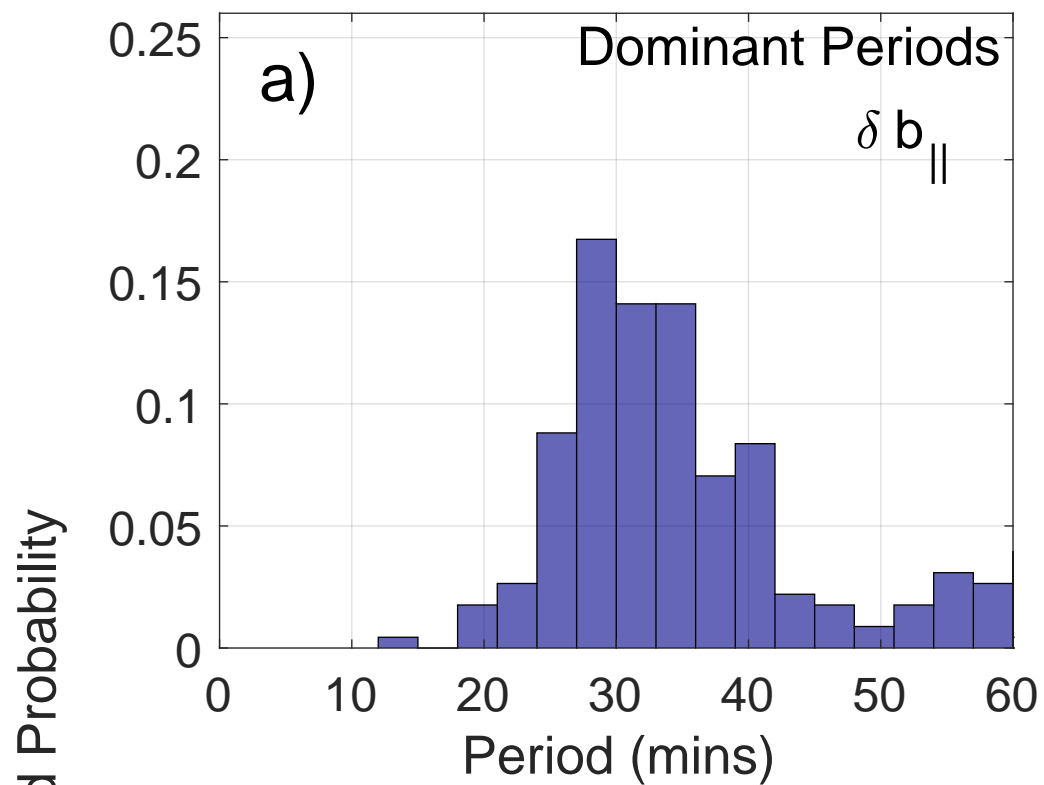


Figure.

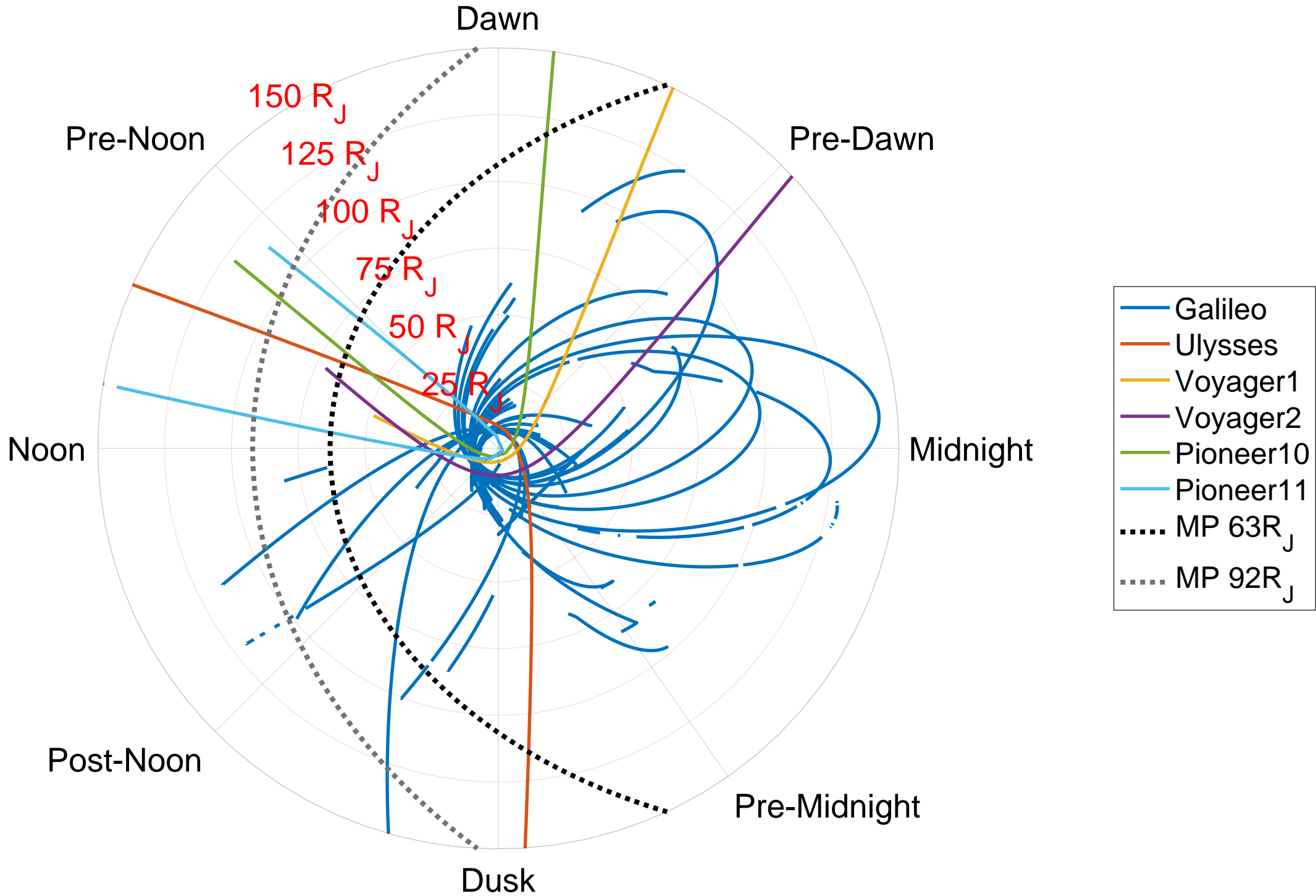
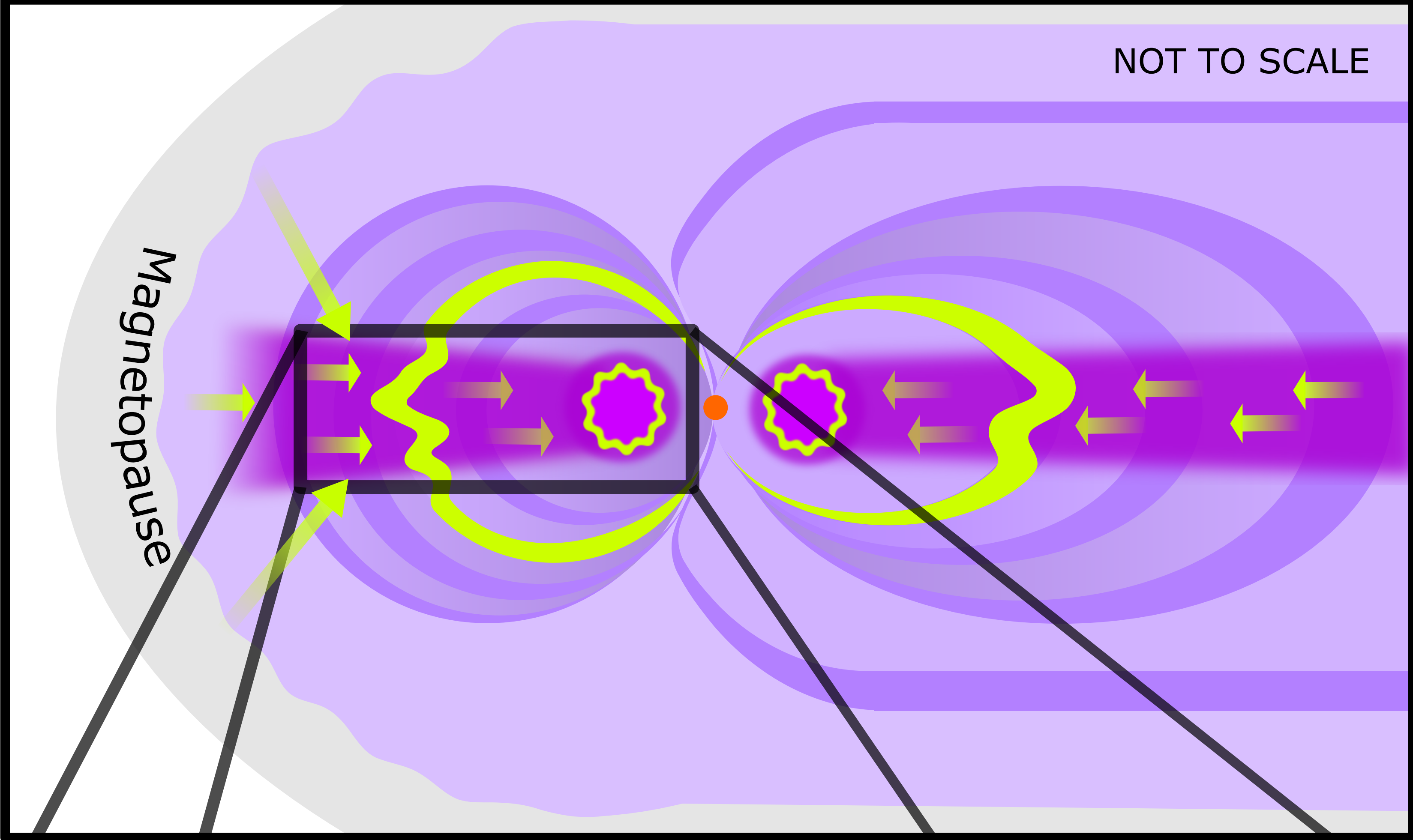


Figure.

NOT TO SCALE

Magnetopause



NOT TO SCALE

SAWs

Plasma Torus

Fast-Mode Waves

Torus Resonance

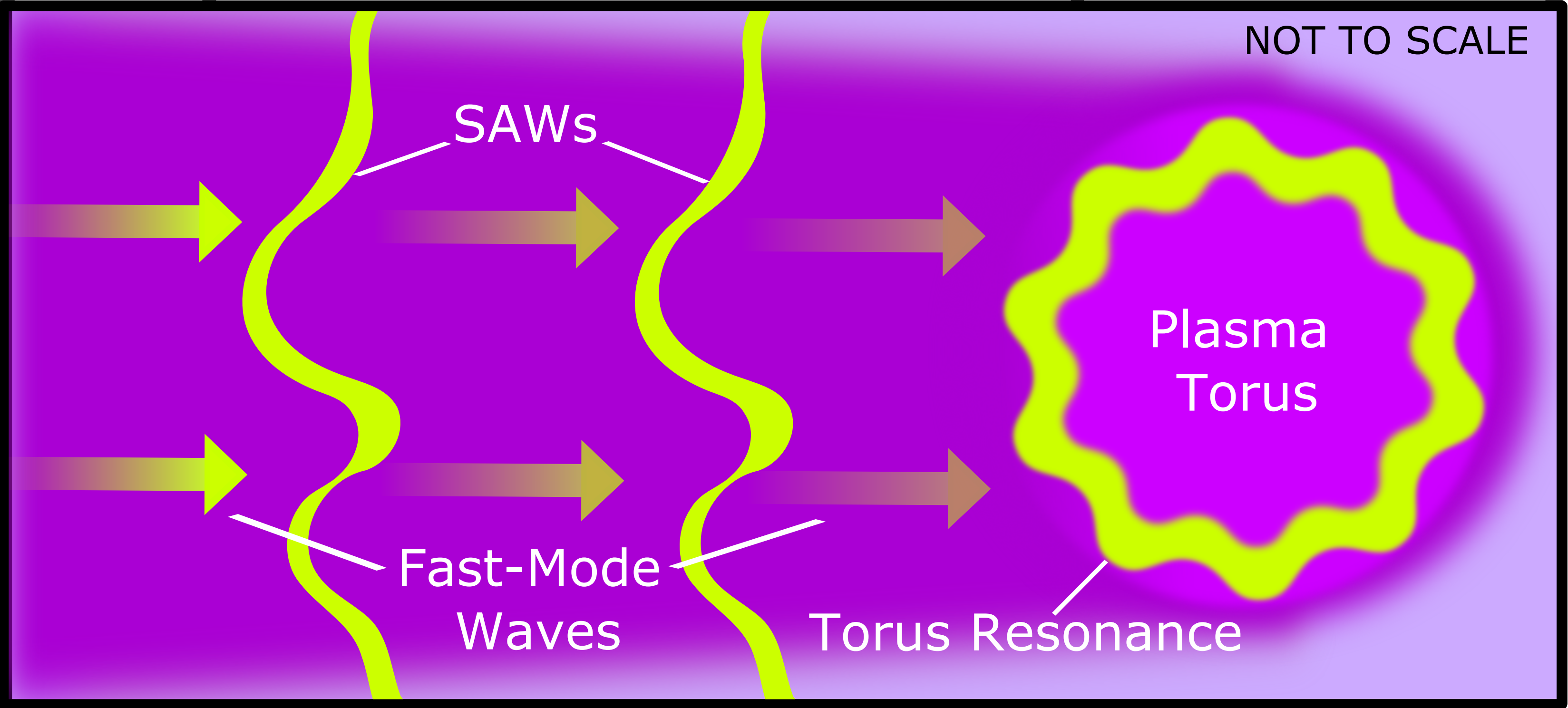


Figure.

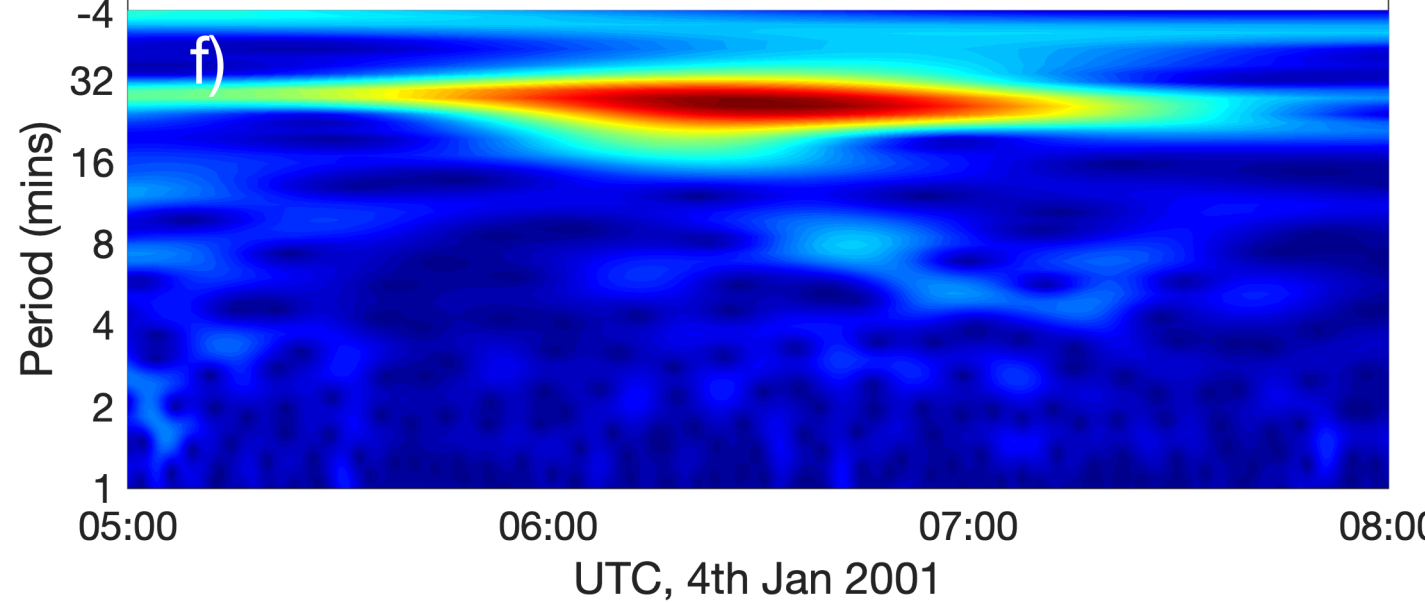
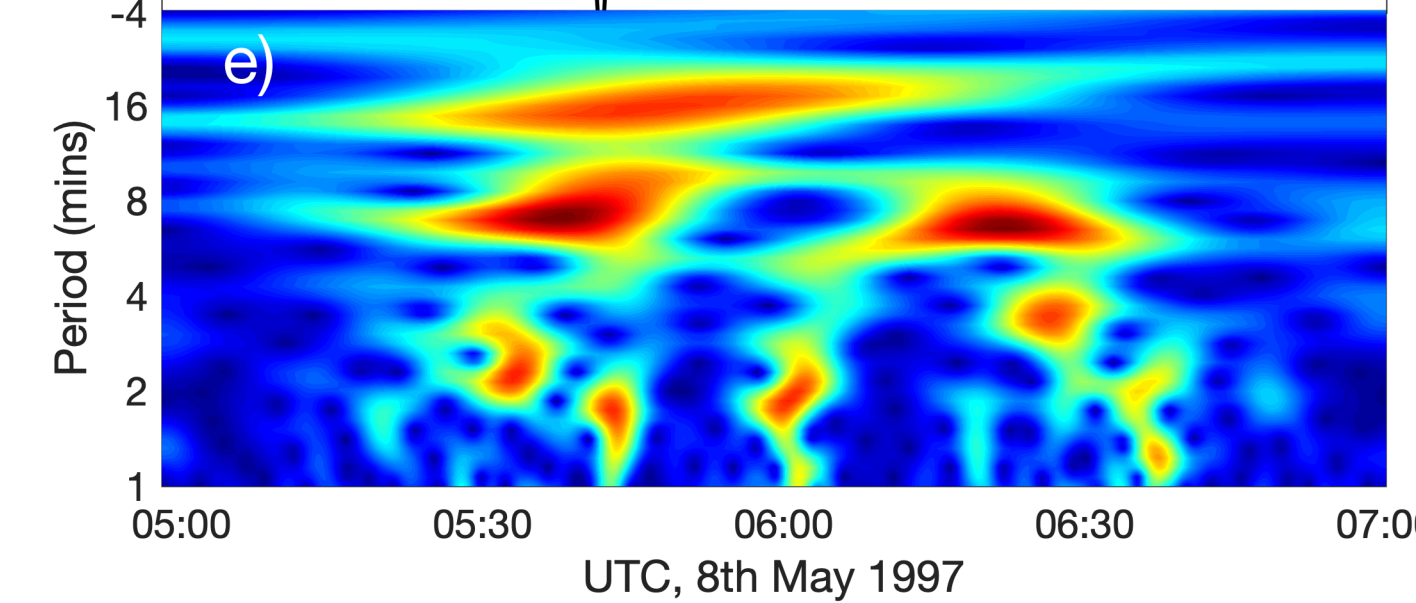
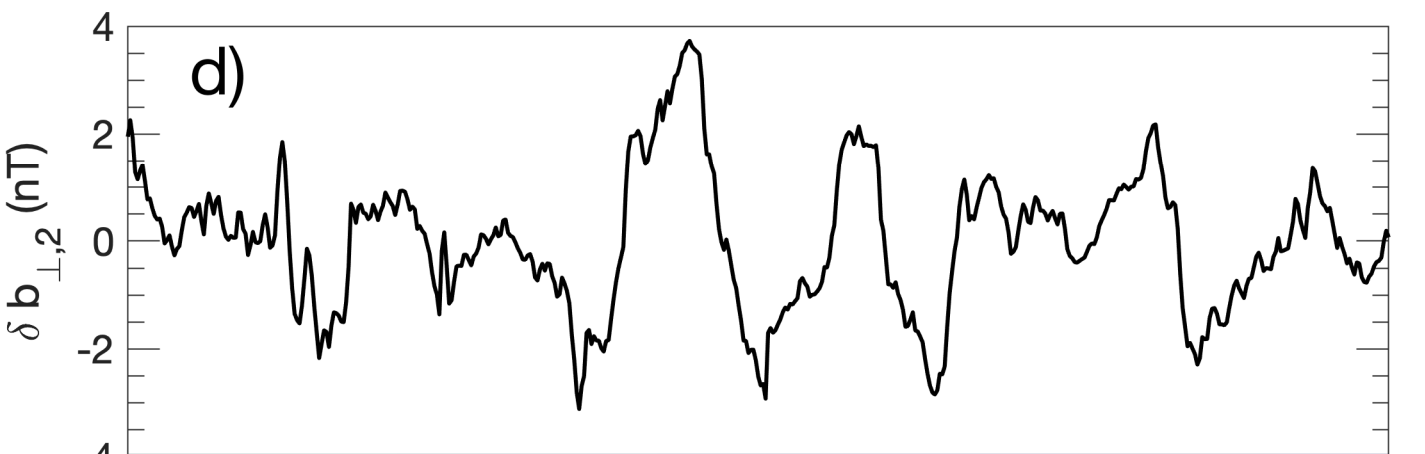
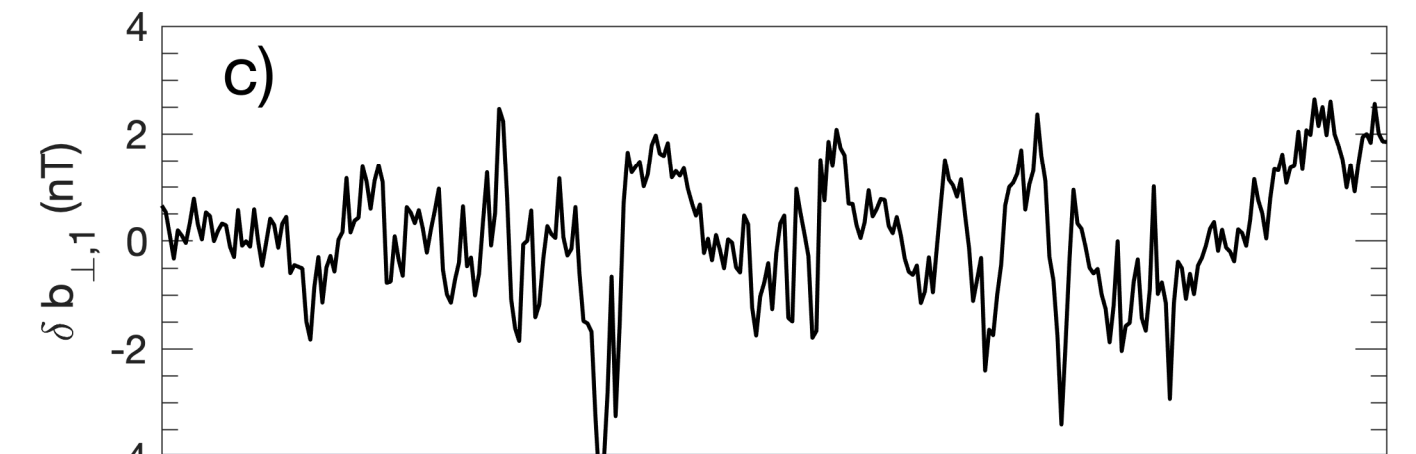
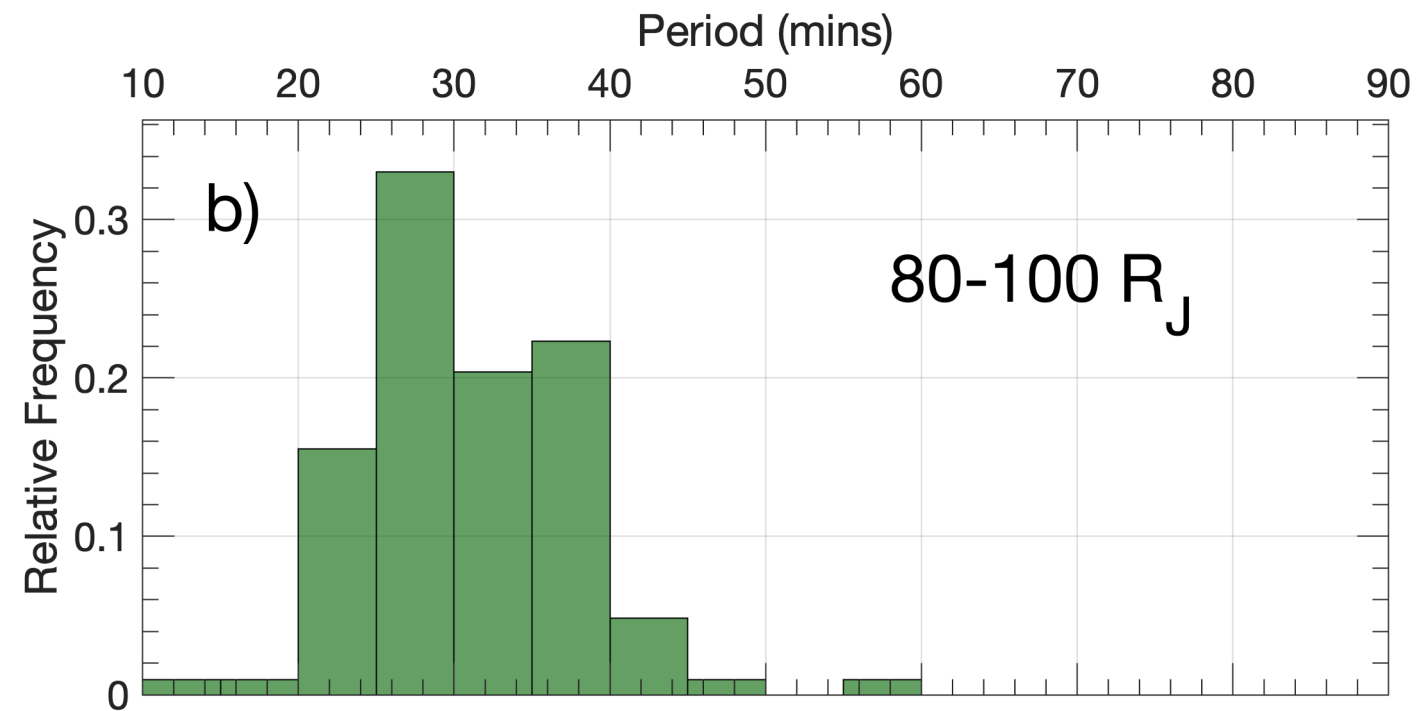
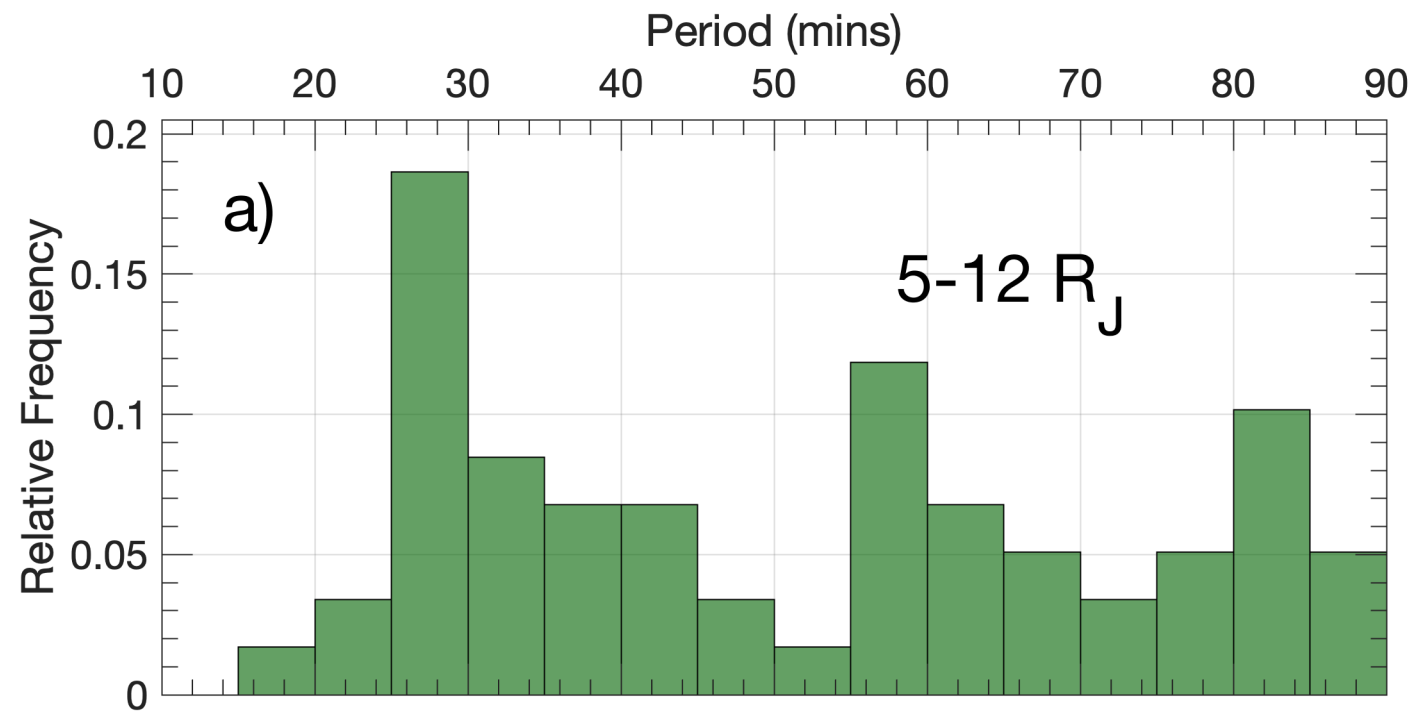


Figure.

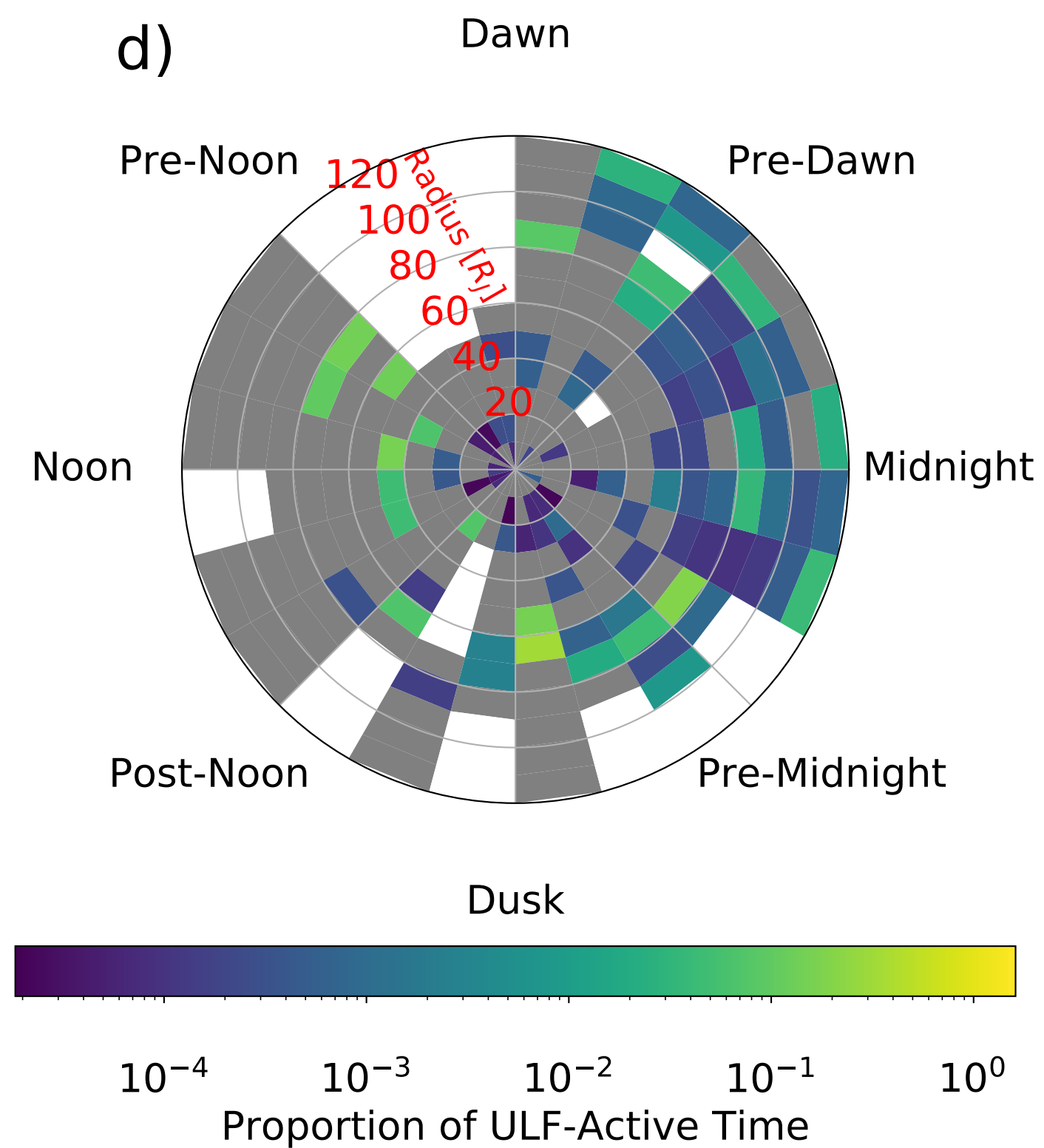
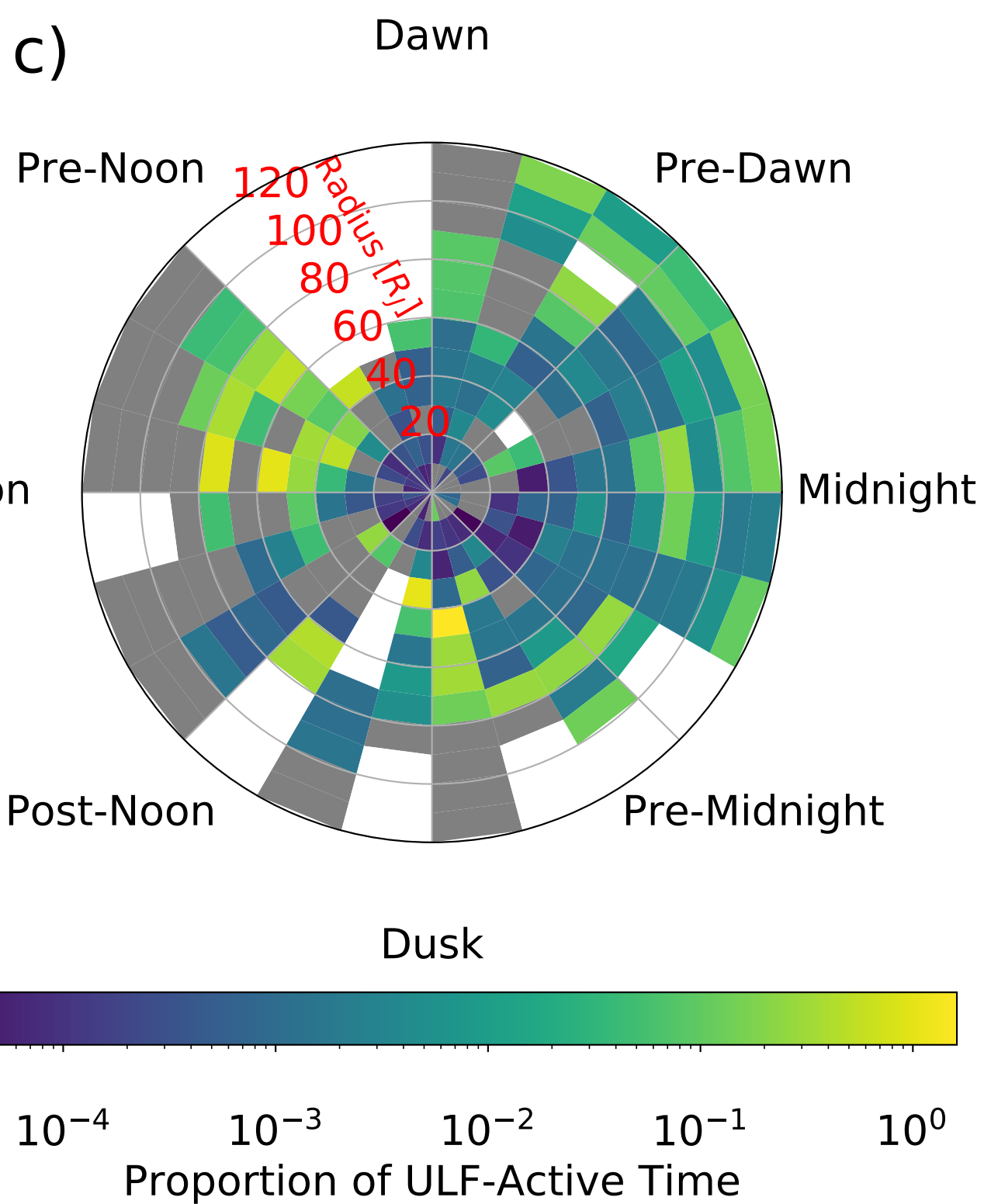
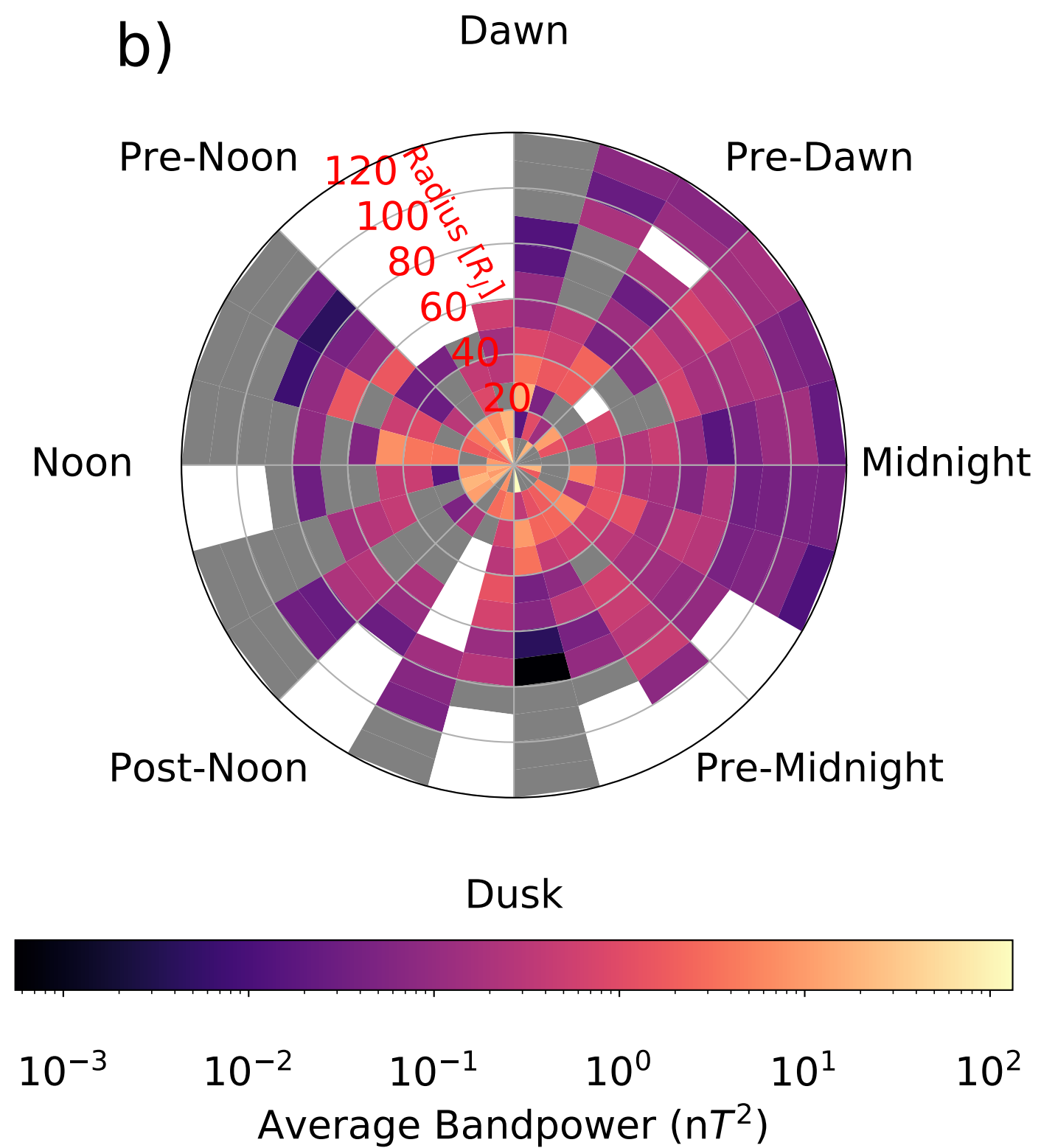
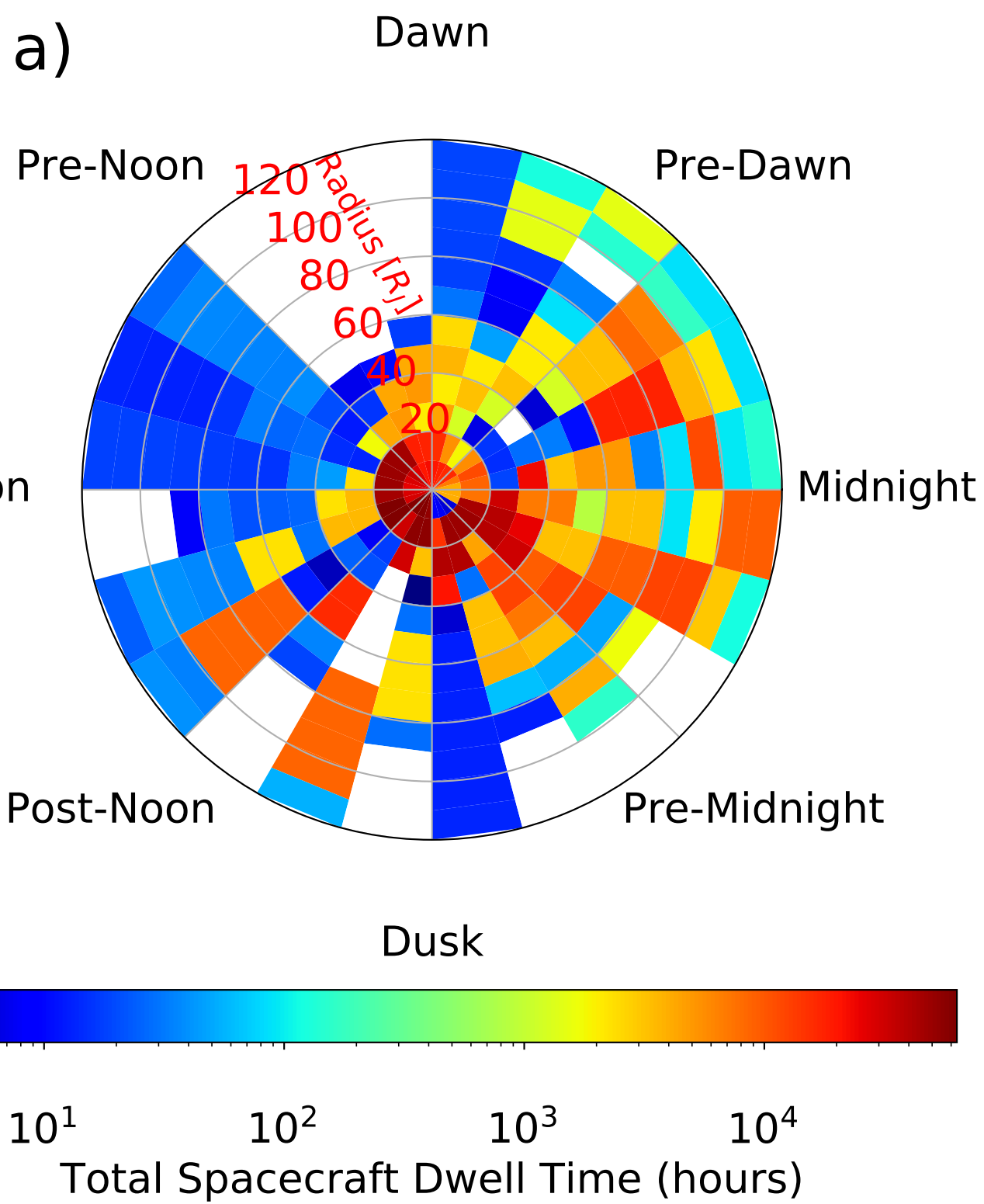
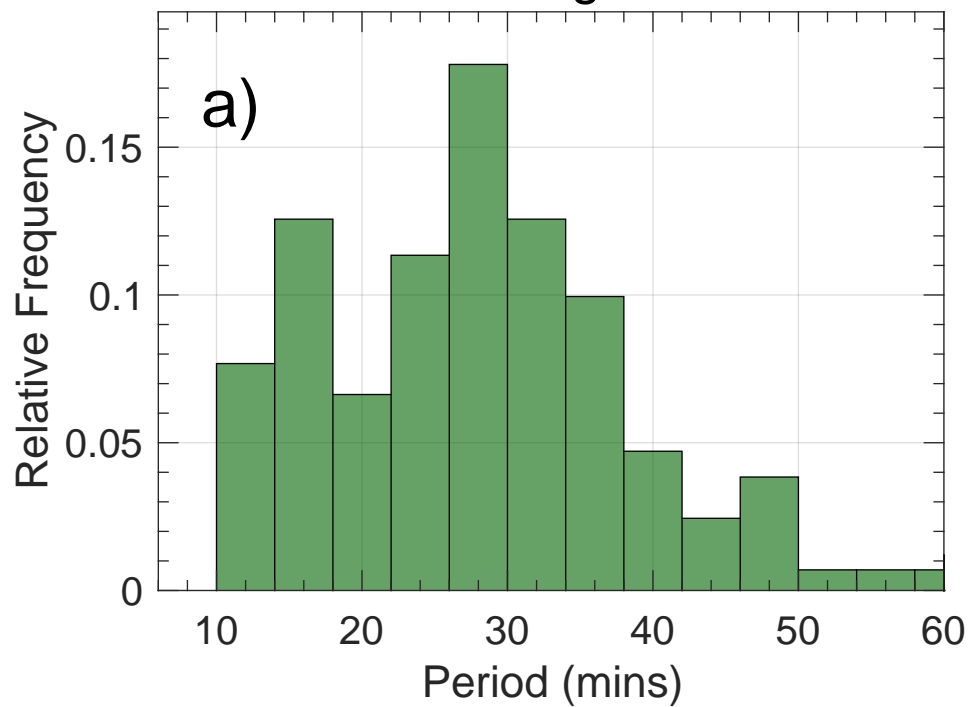
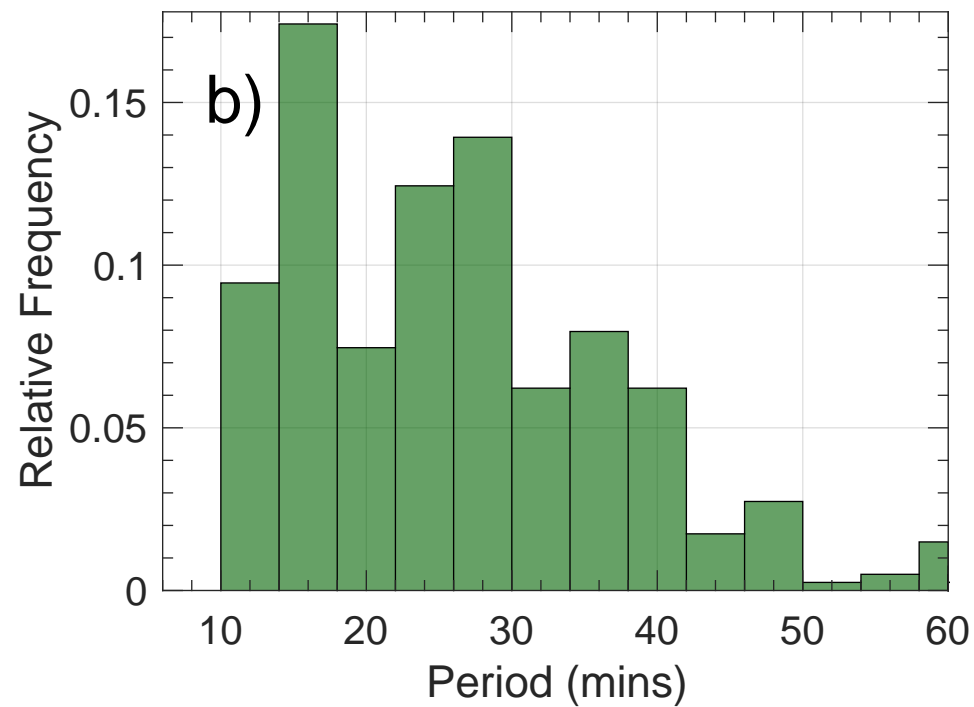


Figure.

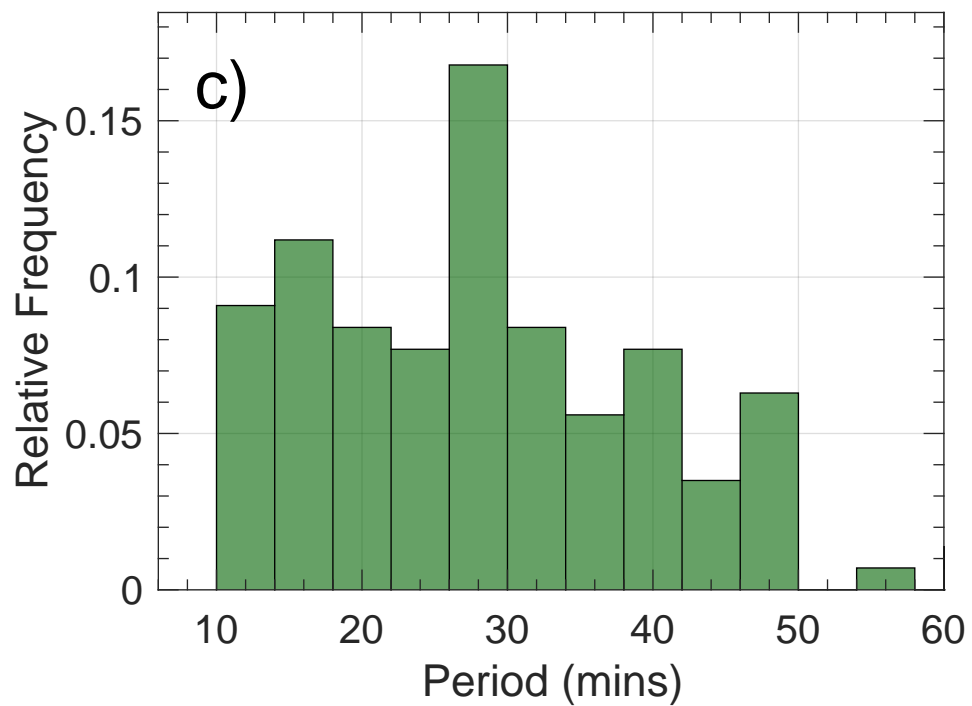
Midnight



Dawn



Noon



Dusk

